Concordance of White Matter and Gray Matter Abnormalities in Autism Spectrum Disorders: A Voxel-Based Meta-Analysis Study

Franco Cauda,[1,2]* Tommaso Costa,[2] Sara Palermo,[2] Federico D'Agata,[1,2] Matteo Diano,[1,2] Francesca Bianco,[3] Sergio Duca,[1] and Roberto Keller[3]

[1]*CCS fMRI, Koelliker Hospital, Turin, Italy*
[2]*Department of Psychology, University of Turin, Turin, Italy*
[3]*Adult Autism Center, ASL To2, Turin, Italy*

Abstract: There are at least two fundamental unanswered questions in the literature on autism spectrum disorders (ASD): Are abnormalities in white (WM) and gray matter (GM) consistent with one another? Are WM morphometric alterations consistent with alterations in the GM of regions connected by these abnormal WM bundles and vice versa? The aim of this work is to bridge this gap. After selecting voxel-based morphometry and diffusion tensor imaging studies comparing autistic and normally developing groups of subjects, we conducted an activation likelihood estimation (ALE) meta-analysis to estimate consistent brain alterations in ASD. Multidimensional scaling was used to test the similarity of the results. The ALE results were then analyzed to identify the regions of concordance between GM and WM areas. We found statistically significant topological relationships between GM and WM abnormalities in ASD. The most numerous were negative concordances, found bilaterally but with a higher prevalence in the right hemisphere. Positive concordances were found in the left hemisphere. Discordances reflected the spatial distribution of negative concordances. Thus, a different hemispheric contribution emerged, possibly related to pathogenetic factors affecting the right hemisphere during early developmental stages. Besides, WM fiber tracts linking the brain structures involved in social cognition showed abnormalities, and most of them had a negative concordance with the connected GM regions. We interpreted the results in terms of altered brain networks and their role in the pervasive symptoms dramatically impairing communication and social skills in ASD patients. *Hum Brain Mapp 35:2073–2098, 2014.* **© 2013 Wiley Periodicals, Inc.**

Key words: autism spectrum disorder; white matter changes; gray matter changes; VBM; DTI; ALE meta-analysis

INTRODUCTION

Autism spectrum disorders (ASD) are a group of neurodevelopmental pathologies characterized by impairments in language, quality of communication, and social skills as well as by repetitive and stereotypic patterns of behavior, appearing before 3 years of age [DSM IV-TR, APA 2000]. Categorical diagnoses [DSM IV-TR, APA 2000] represent only an approximation to the real clinical complexity of ASD, a dimensional continuum which can range from minimal autistic traits to full-blown autism and from severe

Additional Supporting Information may be found in the online version of this article.

*Correspondence to: Dr. Franco Cauda, Department of Psychology, Via Po 14, Turin 10123, Italy. E-mail: franco.cauda@unito.it

Received for publication 18 June 2012; Revised 18 March 2013; Accepted 2 April 2013.

DOI: 10.1002/hbm.22313

Published online 26 July 2013 in Wiley Online Library (wileyonlinelibrary.com).

mental retardation to high-functioning autism or Asperger's disorder with normal or high IQ [e.g., Piven et al., 1997; Sacco et al., 2010]. In most cases, developmental abnormalities later leading to autism begin prenatally, reducing apoptosis and/or boosting cell proliferation, and affecting cell migration, differentiation, and synaptogenesis [Persico and Bourgeron, 2006; Rutter, 2011]. An investigation of cerebral changes in ASD is thus crucial for a deep understanding of the pathology and has strong implications for both etiological and diagnostic issues.

Over the last decade, the application of neuroimaging techniques has played an important role in increasing knowledge about structural brain organization in ASD compared to normal development [Anagnostou et al., 2011; Pina-Camacho et al., 2012]. Voxel-based morphometry (VBM), a computational based technique that measures focal differences in concentrations of brain tissue [Ashburner and Friston, 2000], has provided new insights into the changes in brain structures associated with ASD [Radua et al., 2011]. Specifically, white and gray matter (WM; GM) changes have been detected throughout the brain, in regions such as the hippocampus and parahippocampal areas, the fusiform and the cingulate gyri, the cerebellum, the corpus callosum, the internal capsule, and the caudate [Boddaert et al., 2004; Bonilha et al., 2008; Ke et al., 2008, 2009; McAlonan et al., 2005, 2008]. Recently, we conducted a quantitative meta-analysis of these VBM data [Cauda et al., 2011], and showed that ASD is due to changes in multiple, spatially distributed networks, including the entire limbic system, the frontostriatal system, the frontotemporal and the frontoparietal networks, and the cerebellar system. Besides, diffusion tensor imaging (DTI), a technique that measures local water molecular displacement [Le Bihan et al., 2001], can provide data about WM connections between brain regions. DTI has provided evidence about impaired network structural connectivity in ASD, which has been correlated to social, communication, or behavioral deficits [Ke et al., 2009].

Various clues suggest that related neural regions may vary mutually, with morphometric changes in the same or reverse direction in healthy and pathological populations [Douaud et al., 2007; Hua et al., 2009; Phillips et al., 2011; Ruef et al., 2012; Xu et al., 2009], due to reciprocally trophic effects mediated by direct axonal connections [Gong et al., 2012; Mechelli et al., 2005; Nosarti et al., 2008]. It is important to emphasize that, although the morphology of the human cortex varies remarkably across individuals, regardless of overall brain size, this variability shows similar patterns among different cerebral regions, implying a structural interaction/association [Mechelli et al., 2005]. Indeed, GM density in a region is a good predictor of the density of the homotopic region in the contralateral hemisphere across the adult population [Mechelli et al., 2005]. Lerch et al. [2006] also found significant interregional thickness correlations within the cerebral cortex. Interestingly, altered patterns of interregional thickness correlations have been found in Alzheimer's disease [He et al., 2008] and multiple sclerosis [He et al., 2009]. These findings suggest that cortical thickness correlations between two different regions may reflect the underlying level of structural and functional integrity of their fiber connection; this leads to the expectation of a convergence between morphological and connectivity measures. Indeed, Lerch et al. [2006] showed that the correlation maps of cortical thickness measured using Broca's area (BA 44) as a seed region, bear a striking resemblance to the DTI tractography maps of the arcuate fasciculus. Similarly, using cortical thickness correlation measurements between brain regions, He et al. [2008] reported significant short- and long-range connections in both the intra and interhemispheric regions, many of which were consistent with known neuroanatomical pathways obtained from human DTI data. However, to the best of our knowledge, the actual kind of relationship between thickness correlation and underlying anatomical connectivity is still unclear. Gong et al. [2012] hypothesized that a trophic effect via direct axonal connections could result in thickness changes in the same direction, while functional connectivity between antagonist regions could result in divergences between thickness correlation and diffusion connections.

This study was performed to investigate concordance between GM and WM modifications in ASD through a meta-analytic approach taking into account VBM and DTI data. We intend to answer some fundamental questions. Are abnormalities in WM and GM consistent with one another? Are WM morphometric alterations consistent with alterations in the GM of areas connected by these abnormal WM bundles and vice versa? The results should add new useful constraints to ASD interpretation models and accurate diagnosis.

MATERIALS AND METHODS

Selection of Studies

Data on relevant GM changes were taken from the database built for the analysis of the related work published by Cauda et al. [2011]. For details about the selection of these articles, please see the "Materials and Methods" section of that publication.

To carry out a systematic search of relevant articles concerning WM abnormalities in ASD we used two different sets of query terms: on one side "autism" and "voxel-based morphometry," on the other "autism" and "diffusion tensor imaging." Using PubAtlas (www.pubatlas.org), an association explorer program that acts as a front-end to PubMed, we found a co-occurrence among the first set of query terms, measured by the natural logarithm of the Jaccard Index, equal to −6.11, and a co-occurrence among the second set of query terms equal to −5.8. Accordingly, up until August 2011, only 87 papers had been indexed on PubMed with the selected search terms. We also searched the bibliographies of published meta-

analyses and reviews on ASD to identify additional studies which were not included in the PubMed literature search database. All included articles were analyzed and any that did not meet the inclusion criteria were excluded. Inclusion criteria were (a) studies including GM and WM locations in Talairach/Tournoux or Montreal Neurological Institute (MNI) coordinates; (b) studies in which the field of view was not confined to a restricted region of the cortex (ROI) but addressed the whole brain; (c) studies including a group comparison between ASD vs. healthy subjects; (d) studies with well specified VBM/DTI analysis; and (e) only original contributions. We also tried to identify any instances of multiple reporting of single data sets across articles, to ensure that only one report of each study contributed to the coordinates included in the present meta-analysis (see Supporting Information Fig. S1). Following the recommendations provided by Moher et al. [2010], we used tables to collect a detailed description of neuroimaging data acquisition modalities, VBM/DTI techniques and data referring to the number of increases and decreases in GM and WM foci (Table I). We also checked the clinical condition of the sample in terms of adherence to diagnostic criteria for ASD, any comorbidity, medication, and the overlap of control groups and clinical samples (Table II). Based on these criteria, 23 papers were included (see Supporting Information Fig. S1) with a total of 1,196 subjects (575 patients and 621 controls). The average age was 18.12 years for the group of patients and 16.89 for the control group; the average IQ was 96.37 for patients and 108.32 for controls.

For the sake of accuracy, the sample of subjects on which the previous analysis of the GM was based was composed of 728 subjects (350 ASD and 378 controls). This previous ASD group included subjects with a diagnosis of high-functioning autism (HFA) (66 subjects), ASP (86 subjects), and 198 with an unspecified diagnosis.

Activation Likelihood Estimation (ALE)

We used ALE meta-analysis, a quantitative voxel-based meta-analysis method [Laird et al., 2005; Lancaster et al., 2000, 2007], to estimate consistent activation across all the selected studies.

In ALE, 3-D coordinates in stereotactic space are pooled from a number of like studies. Each reported coordinate (focus) is modeled by a 3-D Gaussian distribution defined by a user-specified parameter (the full-width half-maximum, FWHM). More specifically, for each reported coordinate (focus) the probability that the focus is located in the voxel is given by:

$$p_i = \frac{e^{-d_i^2/2\sigma^2}}{(2\pi)^{3/2}\sigma^3}\Delta V$$

where d_i is the distance between the focus taken into consideration and all the other voxels and σ is the standard deviation of the Gaussian.

To obtain the probability for the entire voxel volume, the Gaussian is multiplied by the volume of the voxel ΔV.

To take the random effect into account, the FWHM was selected using the modified ALE algorithm [Eickhoff et al., 2012] that provides a quantitative estimate of between-subjects and between-template variability explicitly modeling the spatial uncertainty in the reported coordinate.

Thus, the FWHM is calculated using the parameter reported in [Eickhoff et al., 2009], as:

$$\mathrm{FWHM}_{\mathrm{effective}} = \sqrt{(\mathrm{FWHM}_{\mathrm{template}})^2 + \left(\frac{\mathrm{FWHM}_{\mathrm{subj}}}{\sqrt{\mathrm{N}_{\mathrm{subj}}}}\right)^2}$$

These modeled probabilities are then combined across foci for each experiment resulting in a modeled activation (MA) map for each experiment.

Subsequently, voxelwise ALE scores are computed by taking the union of the MA maps $1-\prod_i^{N_{\mathrm{foci}}}(1-p(i))$, where $p(i)$ is the probability associated with the ith focus at this particular voxel, to estimate the convergence across experiments at each voxel. To distinguish "real" convergence from random convergence, ALE scores are compared to an empirical null-distribution reflecting a random spatial association between experiments. Hereby, a random-effects inference is based on the above-chance convergence between experiments. Computationally, this null-hypothesis is derived by sampling a voxel at random from each of the MA maps and taking the union of these values in the same manner as done before for the voxels in the analysis. The P-value of a "real" ALE score is then given by the proportion of equal or higher values obtained under the null-distribution. Results for each meta-analysis were then thresholded at cluster level ($P < 0.05$ familywise error [FWE] corrected).

ALE maps were computed using a Java-based version of the ALE software named GingerALE (version 2.1.1) and custom Matlab routines at an FDR-corrected threshold of $P < 0.05$ and a minimum cluster size of $K > 100$ mm^3.

JackKnife Analysis

To rule out the possibility of some activations being driven by the involvement of a small subset of studies, we performed a jackknife analysis. This is a non-parametric method for estimating the sampling distribution of a statistic [Amanzio et al., in press; Radua and Mataix-Cols, 2009; Radua et al., 2010]. Given a sample data set and a desired statistic, the jackknife works by computing the desired statistic with an element deleted. This is done for each element of the data set. These statistics are gathered to estimate the sampling distribution. The results are presented as probability maps where a high probability means that a certain region is driven by the majority of the experiments included. On the contrary, a low probability means that a certain region is driven by few

TABLE I. Overview of the included studies

	Study[a]		VBM technique			DTI technique						Morphological changes foci	
	Year	First Author	VBM	VBM algorithm	Voxel size (mm)	DTI	FOV (cm^2)	Slice thickness	Smoothing (mm)	Original coordinates	Scanner	WM_ increase	WM_ decrease
DTI	2004	Barnea-Goraly et al.				SPM99	24	5 mm/skip 1.5 mm	4	TAL	3T	0	6
	2007	Keller et al.				SPM2	20	3 mm	8	MNI	3T	0	5
	2009	Cheung et al.				SPM2	28	5 mm/skip 1.5 mm	6	TAL	1.5T	2	7
	2009	Pardini et al.				FDT	22.4	2 mm	4	MNI	3T	0	11
	2010	Cheng et al.				FSL 4.1	26	2.2 mm		MNI	1.5T	16	3
	2010	Noriuchi et al.				IDL		2 mm	6	MNI	3T	0	8
	2011a	Jou et al.				FSL/TBSS	24	2.5 mm		MNI	3T	0	3
	2011b	Jou et al.				BioImage Suite	25.6	4 mm		TAL	1.5T	0	12
VBM	2002	McAlonan et al.	SmaRT on SPARC	Modulated volume	2.2 mm^3					TAL	1.5 T	4	4
	2004	Boddaert et al.	SPM99	Optimized	1.2 thick				12	TAL	1.5 T	0	2
	2005	McAlonan et al.	BAMM on SPARC	Segmentation	3 thick				4.4	TAL	1.5 T	0	2
	2005	Waiter et al.	SPM2	Optimized	1 mm^3				8	TAL	1.5 T	0	24
	2006	Spencer et al.	SPM99	Optimized adaptation	1.7 mm^3				12	TAL	1.5 T	1	1
	2007	Craig et al.	SPM2	Optimized	1.5 thick				5	TAL	1.5 T	5	3
	2008	Bonilha et al.	SPM5	Optimized	1 mm^3				10	MNI	2T	0	43
	2008	Ke et al.	SPM5	Optimized	2 thick				8	TAL	1.5 T	0	2
	2009	Ke et al.	SPM5	Optimized	2 thick				8	TAL	1.5 T	3	6
	2009_exp A	McAlonan et al.	BAMM on SPARC	Segmentation	3 thick				4.4	TAL	1. 5 T	2	1
	2009_exp B	McAlonan et al.	BAMM on SPARC	Segmentation	3 thick				4.4	TAL	1.5 T	2	1
	2010	Ecker et al.	SPM5	Segmentation	1.1 thick				8	TAL	3T	9	9
	2010	Hyde et al.	CIVET	Modulated concentration	1 mm^3				12	MNI	3T	0	3
	2010_exp A	Toal et al.	SPM2	Optimized	~1 mm^3				8	TAL	1.5 T	0	2
	2010_exp B	Toal et al.	SPM2	Optimized	~1 mm^3				8	TAL	1.5 T	0	6
	2010_exp C	Toal et al.	SPM2	Optimized	5 thick				8	TAL	1.5 T	0	2
	2011	Mengotti et al.	SPM5	Modulated volume	1.1 thick				8	MNI	1.5 T	5	0
	2012	Calderoni et al.	DARTEL	Modulated					8	MNI	1.5 T	0	1

[a]Selected studies.

TABLE II. Demographics of the included studies

Study[a]			Sample						Controls				
	Year	First author	Subjects	Age (years)	Range (Years)	♂/♀	Diagnosis	IQ	Subjects	Age (years)	Range (years)	♂/♀	IQ
DTI	2004	Barnea-Goraly et al.	7	14.6 ± 3.4	—	7/0	HFA	101 ± 12.2	9	13.4 ± 2.8	—	7/0	107 ± 8.5
	2007	Keller et al.	34	18.9 ± 7.3	10–35	34/0	HFA	102 ± 14.8	31	10.9 ± 6.2	10–35	31/0	109.5 ± 9
	2009	Cheung et al.	14	—	6–14	—	—	—	14	—	6–14	—	—
	2009	Pardini et al.	10	19.7 ± 2.83	19–27	10/0	PDD	—	10	19.9 ± 2.64	18–26	10/0	—
	2010	Cheng et al.	25	—	10–18	25/0	ASD	101.6 ± 19.91	25	—	11–18	25/0	109.04 ± 9.45
	2010	Noriuchi et al.	7	13.96 ± 2.68	—	6/1	3HFA; 4ASP	92.71 ± 6.68	7	13.36 ± 2.74	—	6/1	116.43 ± 9.5
	2011a	Jou et al.	15	10.9 ± 3.7	4.9–17	—	ASD	—	8	11.5 ± 2.6	8.9–16.7	—	—
	2011b	Jou et al.	10	13.5 ± 4	8–19	10/0	4AD; 4AS; 2PDD	—	10	13.5 ± 4	8–19	10/0	—
VBM	2002	McAlonan et al.	21	32±10	—	19/2	ASP	—	24	33 ± 7		22/2	—
	2004	Boddaert et al.	21	9.3 ± 2.2	7–15	16/5	Primary autism	55.8 ± 15.8	12	10.8 ± 2.7	7–15	7/5	—
	2005	McAlonan et al.	17	12 ± 1.8	8–14	16/1	Primary autism	101 ± 10	17	11 ± 1.2	8–14	16/1	114 ± 14.1
	2005	Waiter et al.	15	15.2 ± 2.2	12–20	15/0	ASD	100.5 ± 19.7	16	15.5 ± 1.6	—	16/0	99.7 ± 18.3
	2006	Spencer et al.	63	16 ± 1.9	13–22	34/29	ASD	59.7 ± 7.7	72	16.7 ± 2.1	13–22	34/38	101.3 ± 15.9
	2007	Craig et al.	14	37.9±11.4		0/14	10 ASP; 4 ASD	103.4±17	19	35±14	—	0/19	111.2±14.5
	2008	Bonilha et al.	12	12.4 ± 4	8–23	12/0	AS	—	16	13.2 ± 5	—	16/0	
	2008	Ke et al.	17	8.88 ± 1.96	6–14	14/3	HFA	108.76 ± 19.07	15	9.73 ± 1.67	6-14	12/3	109.8 ± 19.22
	2009	Ke et al.	12	8.75 ± 2.26	—	24/0	12 HFA	100.6 ± 18.79	10	9.4 ± 2.07	—	10/0	99.83 ± 17.93
	2009_exp A	McAlonan et al.	18	11.2 ± 2.5	—	15/3	ASP	—	55	10.7 ± 2.7	—	47/8	
	2009_exp B	McAlonan et al.	18	11.6±3	—	15/3	ASD	—	55	10.7±2.7	—	47/8	
	2010	Ecker et al.	22	27 ± 7	—	22/0	ASD	104 ± 15	22	28 ± 7	18–42	22/0	111 ± 10
	2010	Hyde et al.	15	22.7 ± 6.4	—	15/0	AS	100 ± 13	15	19.2 ± 5	—	15/0	107 ± 12
	2010_exp A	Toal et al.	65	31 ± 10	16–59	56/9	39 ASP; 26 AS	98 ± 21	33	32 ± 9	19–58	30/3	105 ± 12
	2010_exp B	Toal et al.	39	32 ± 12	16–59	35/4	ASP	106 ± 15	33	32 ± 9	19–58	30/3	105 ± 12
	2010_exp C	Toal et al.	26	30 ± 8	16–59	21/5	AS	84 ± 23	33	32 ± 9	19–58	30/3	105 ± 12
	2011	Mengotti et al.	20	7 ± 2.25	4–14	18/2	AS	—	22	7.68 ± 2.03	4–11	20/2	—
	2012	Calderoni et al.	38	53 ± 18 months	25–88 months	0/38	22AD; 16 PDD	—	38	—	—	0/38	—

[a]Selected studies.

experiments thus indicating the need for caution in interpreting such data.

Multidimensional Scaling

We used multidimensional scaling to inspect the similarity/sparsity of the results of the studies involved in this meta-analysis. This consisted of transforming the MA maps of each experiment into a series of vectors containing all the values of the voxels of the original matrix [Kriegeskorte et al., 2008]. A representational similarity matrix was then constructed by calculating the correlation between each vector (r). The distance matrix (or representational dissimilarity matrix) was then constructed as $1 - r$. Indeed, multidimensional scaling (MDS) was applied to the distance matrix to provide a geometrical representation of dissimilarities among results. MDS is a technique which finds a low-dimensional projection of points, where it tries to fit the given distances between points as well as possible. By means of this technique, MA maps having a shorter Euclidean distance (the first quartile) were represented as connected by a straight line. A shorter Euclidean distance means greater representational similarity.

Concordance Analysis

The MA maps for GM and WM were submitted to a specifically developed Matlab script that identifies the regions of concordance starting from a topological matrix that describes the connections between WM and GM areas.

Since there are no atlases showing all the connections between human GM and WM, we developed a topological proximity matrix which describes when a GM region and a WM bundle are connected. Subsequently, we submitted the WM and GM ALE results to a script that compares the ALE maps with the topological matrix and produces a table output with the percentage of active voxels in each region. This script was used to iteratively inspect the MA maps to search for statistically significant concordances between WM and GM results.

Topological Proximity Matrix

First, we identified existing anatomical connections between GM and WM. To do so, we created a matrix of topological proximity using the atlas developed by Mori et al. [2008], Oishi et al. [2008] containing 170 labeled areas from a parcellation of the International Consortium for Brain Mapping (ICBM) template non-linearly normalized in the Talairach space. These regions are classified as left and right Deep White Matter (DWM, 28 right and 28 left regions), Superficial White Matter (SWM, 22 right and 22 left areas) or Gray Matter (GM, 35 right and 35 left s) each one with its own code number. We used a script to loop over all the voxels of the atlas image. Hence, we examined and counted the codes of the nearest voxels for each of the previously identified voxels. Specifically, if you consider that the examined voxel has its origin in $(x, y, z) = (0, 0, 0)$, we examined the following voxels (x, y, z): $(\pm1, 0, 0)$; $(0, \pm1, 0)$; $(0, 0, \pm1)$; $(\pm1, \pm1, 0)$; $(0, \pm1, \pm1)$; $(\pm1, 0, \pm1)$; $(\pm1, \pm1, \pm1)$. We summed the counts of the nearest voxels for all the voxels of a region. Prototypically assuming that region 1 was composed of 10 voxels, we summed the counts of all the 10 distributions of the nearest voxels, obtaining a total distribution by way of the total counts of all the region's neighboring voxels. For example, region 1 could have 100 adjacent voxels inside region 3, another 500 inside region 11, and so on. Repeating this procedure for all the 170 identified regions, we obtained several distributions of counts in the neighboring regions. We obviously ignored voxels inside the same region (clearly some voxels inside region 1 had other region 1 voxels as neighboring voxels).

We entered the distributions obtained in a 170×170 matrix with each row corresponding to a region (from 1 to 170) and each column corresponding to the total counts in other neighboring regions. So, in the above example, while row 1 represented region 1, in the cell corresponding to row 1 and column 3 we entered number 100, in row 1 and column 11 we entered number 500, and so on.

To binarize the matrix, we set 1 in the cell when two regions (represented by rows and columns) were significantly connected or 0 when they were not. To judge whether a link was significant, first we divided the counts in each cell by the average number of voxels in the corresponding row and column regions (as the width of the regions could affect the probability of spurious neighbor counts), then we discarded all the results below the 5th centiles of all the normalized counts. The resulting 170×170 topological proximity matrix contains one if two regions (row by column) are neighboring or 0 if not.

Concordance Search

For each significant GM MA map, we cycled all the connected WM bundles (as expressed by the topological matrix) to find WM tracts showing one of the three types of concordances: (i) positive = GM increase and WM increase; (ii) negative= GM decrease and WM decrease; (iii) discordance = GM increase and WM decrease and vice versa.

Specifically, for each labeled region containing an activation the following conditions could occur:

$$z_1 = I(G_i = 1,\ W_j = 1)$$

$$z_2 = I(G_i = 1,\ W_j = 0)$$

$$z_3 = I(G_i = 0,\ W_j = 1)$$

$$z_4 = I(G_i = 0,\ W_j = 0)$$

where $I(.)$ is an indicator function and G and W are the gray and white regions, respectively. This brain atlas passage collapses all the information from voxels into ROIs.

This is a coarse reduction of the information into a binary map. We decided to use this type of binary transformation rather than a probabilistic approach, which includes a blurring of the position of the tracts, because this method could augment the variability and the approximation of the results, considering that the final result is, however, always a binary result on ROIs.

We tested the significance of the resulting network with a Monte Carlo simulation, generating 10,000 undirected random networks with the same number of nodes and edges. The resulting statistics were thresholded at 95%.

Data were visualized with BrainNet (http://www.nitrc.org/projects/bnv/), Cytoscape [Shannon et al., 2003] and Orange Canvas [Curk et al., 2005].

Topological Analysis of the Results

A series of topological measures were computed starting from the network composed of significant concordances. Betweenness centrality, shortest path length, and edge betweenness were calculated and visualized using Cytoscape (http://www.cytoscape.org/).

The betweenness centrality is a measure of a node's centrality in a network; it indicates the load and the importance of a node inside the network. It is related to the number of shortest paths from all vertices that pass through a certain node. Similar to this measure but related to an edge is the edge betweenness. This network measure is defined as "the number of shortest paths between pairs of vertices that run along it."

The shortest path length distribution gives the number of node pairs (n,m) with $L(n,m) = k$ for $k = 1,2,\ldots$. were the shortest path is defined as "the length of the shortest path between two nodes n and m is $L(n,m)$."

Network Clustering

We used the k-core decomposition algorithm [Alvarez-Hamelina et al., 2006; Bader and Hogue, 2003] to disentangle the hierarchical structure of our concordance network by progressively focusing on their central cores. The k-core decomposition of a network "N" works by recursively removing all the vertices of degree less than k, until all vertices in the remaining graph have at least degree k. The algorithm works in three steps: given a graph $G = (V,L)$ with n vertices (V) and 1 edge (L), the first step is node scoring: it computes the degrees of the vertices and orders the set of vertices V in increasing order of degrees, while simultaneously computing the maximum degree. Next, the algorithm assigns higher scores to nodes whose immediate neighbors are more interconnected (highest k-core). It then selects the complex with the highest-scoring node and recursively moves outward including nodes whose scores are above a given threshold. These steps are repeated and then the clusters are filtered by discarding those without at least k-core networks.

This procedure allowed us to cluster our concordance network graph as its central most densely connected subgraph. In our case, the algorithm found a k-core = 2.

RESULTS

Figures 1 and 2 show the dissimilarity matrix and the multidimensional scaling of the MA maps relative to the papers comprised in our meta-analysis. The results of the papers involving a decrease in WM concentration/volume or WM DTI-related parameters, such as Fractional Anisotropy, are rather homogeneous. A wide group of VBM and DTI papers reveal an MA map that converges to a similar spatial representation. Only few studies disclosed results that are eccentric with respect to other studies: for example the papers by Pardini et al. [2009], Bonilha et al. [2008], Waiter et al. [2005], Barnea-Goraly et al. [2004]. Although a minority of the selected papers report WM increases, they exhibit a representational dissimilarity matrix similar to that of papers showing WM decreases.

JackKnife Analysis

The jackknife analysis (Supporting Information Fig. S2) showed all the regions found in the ALE maps that were utilized for this analysis to have high reliability. Regions of concordance are not driven by the involvement of a small subset of studies.

Figure 3 and Supporting Information Table S1 show the ALE results of papers involving a decrease or increase in WM concentration/volume and WM DTI-related parameters. As also suggested by the multidimensional scaling results, the Jackknife analysis showed all the ALE regions to have high reliability (>50%) so all the clusters were included in the subsequent analyses (see Supporting Information Fig. S2).

Results concerning the GM ALE results were discussed in a previous study by the same research group [see Cauda et al., 2011] and are therefore not reported in this article.

Figure 4 and Table III show the concordances between GM and WM results. A significant concordance between GM regions and the corresponding WM fasciculus connecting the two regions is represented through a straight line.

Positive concordances (increase → increase) were found between the right posterior corona radiate and the angular gyrus, and between the left sagittal stratum and the fusiform gyrus, inferior occipital gyrus and middle temporal gyrus (see also Fig. 5, upper and middle panels).

Negative concordances (decrease → decrease) are much more numerous than positive ones. The most represented WM tracts are the corona radiate, the cingulum, the genu of corpus callosum, the right middle cerebellar peduncle, the left internal capsule, the right posterior thalamic

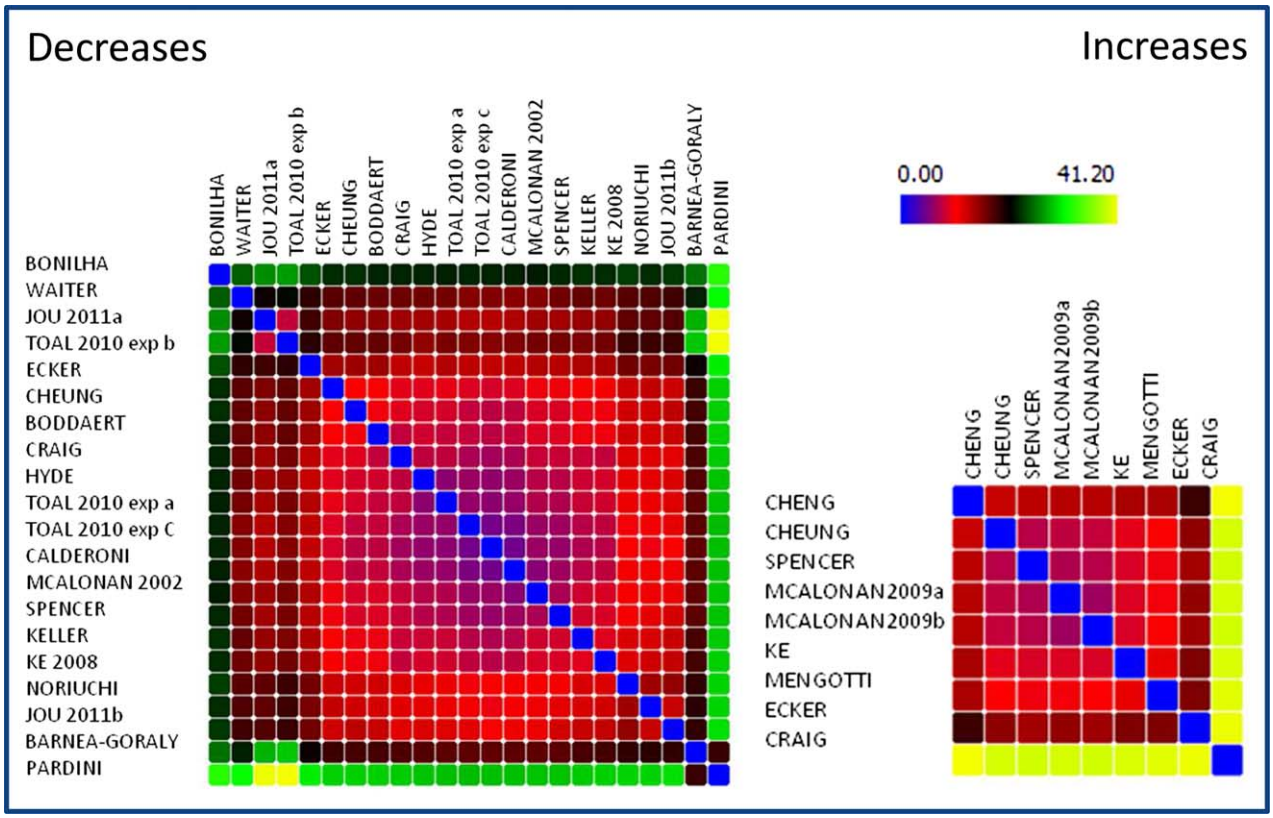

Figure 1.

Representational dissimilarity matrix of the spatial results (MA maps) of the papers involved in the study. Spectrally reordered representational dissimilarity matrix, showing the Euclidean distances between the MA maps of each experiment involved in this meta-analysis. The results are subdivided into WM increases and WM decreases. Low values indicate a high spatial similarity. [Color figure can be viewed in the online issue, which is available at wileyonlinelibrary.com.]

radiation, the right sagittal stratum, the superior longitudinal fasciculus, the right splenium of corpus callosum, and the right superior corona radiate. Among the gray matter structures, we found the left angular gyrus, the right cingulate gyrus, the fusiform gyrus, the right inferior frontal gyrus, the right inferior temporal gyrus, the right insula, the right lingual gyrus, the right middle frontal gyrus, the right middle temporal gyrus, the right parahippocampal gyrus, the right postcentral gyrus, the precentral gyrus, and the superior frontal gyrus (see also Fig. 5, upper and middle panels).

Discordances (decreases → increases) have a similar distribution to that of negative concordances, with only a few differences. Thus they can be ascribed to a compensation mechanism [Dolcos et al., 2002]. Interestingly, most of the discordances follow the results of negative concordances. No GM and only a few WM regions are uniquely detected for discordances: these regions are the bilateral external capsule and the left retrolenticular part of internal capsule (for a better specification of the discordance results see also Fig. 6, Tables IV and V)

While positive concordances are evenly distributed between the two hemispheres (see Fig. 5, lower panels), negative concordances are heavily lateralized on the right side. If we analyze the two major longitudinal tracts separately, we find that the sagittal stratum shows positive concordances on the left side and negative ones on the right side. Conversely, the superior longitudinal fasciculus shows bilateral negative concordances that are denser on the left side.

Figure 7 shows a different view of the nodes and edges represented in Figure 4. This image shows a series of topological measures of the network composed of significant concordances: node dimension indicates betweenness centrality; node color indicates the average shortest path length; edge color and dimension indicate the edge betweenness.

Regions with the highest centrality among the concordances are, on the right side, the insula, the superior longitudinal fasciculus, sagittal stratum, the anterior cingulate and the precentral gyrus, and, on the left side, the superior longitudinal fasciculus, the sagittal stratum supramarginal

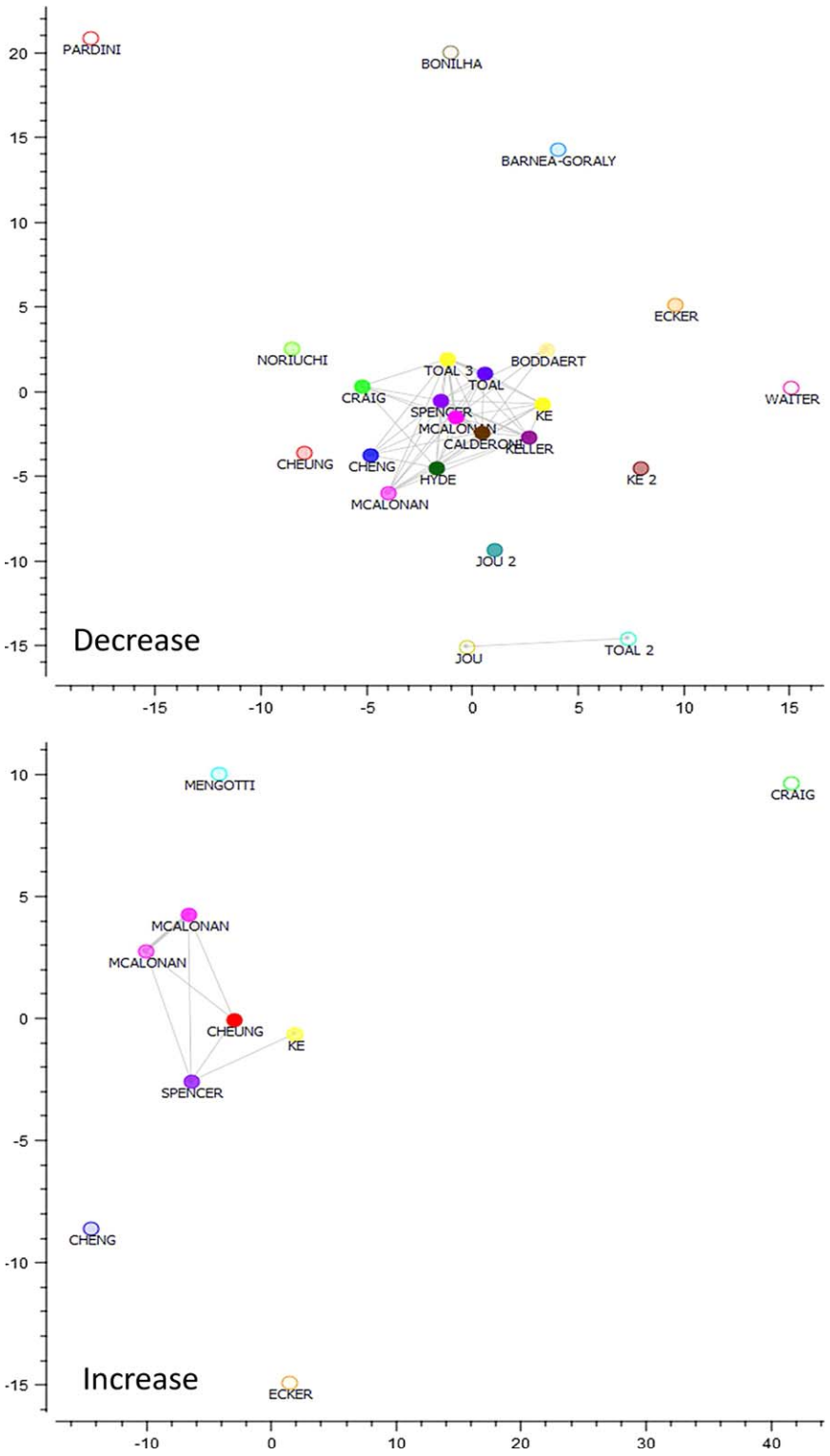

Figure 2.

Multidimensional scaling of the spatial results (MA maps) of the papers involved in the study. Multidimensional scaling of the modeled activations of the papers involved in this study, papers with more similar spatial results (first quartile) are connected by a straight line. Points are color coded on the basis of the paper that each point represents. [Color figure can be viewed in the online issue, which is available at wileyonlinelibrary.com.]

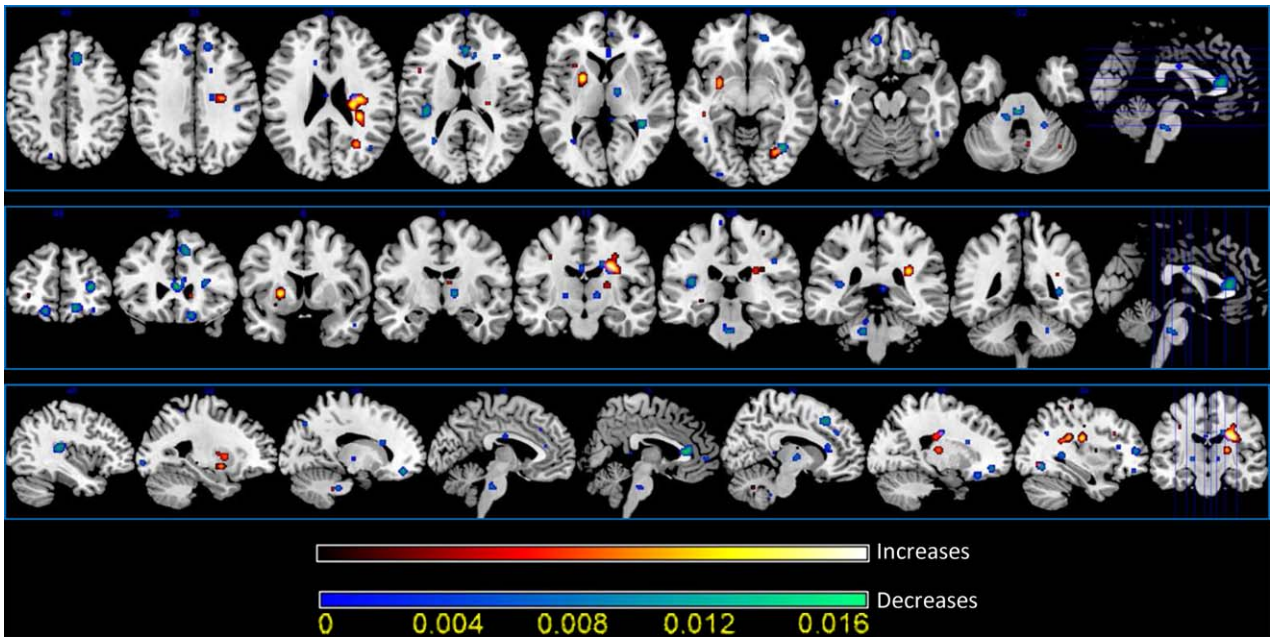

Figure 3.

White matter activation likelihood estimation (ALE) results. Colors from red to yellow show wm increases, colors from blue to green show WM decreases (two-dimensional ALE maps were computed at a false discovery rate corrected threshold of $P < 0.05$, with a minimum cluster size of $K > 100$ mm^3 and visualized using MRIcron). [Color figure can be viewed in the online issue, which is available at wileyonlinelibrary.com.]

gyrus, the middle temporal gyrus, the posterior thalamic radiation, and the precentral gyrus. Most of these regions also have some of the shortest path lengths.

On the right side, tracts showing higher edge betweenness are connected principally to the insular cortex.

A *K*-core clusterization of the concordance results (see Fig. 8) [Alvarez-Hamelina et al., 2006] shows that two densely connected clusters are present in our data: one in the left hemisphere including the fusiform gyrus, the middle temporal gyrus, and the inferior occipital gyrus. The other cluster is in the right hemisphere and includes the superior, middle and inferior frontal gyri, the cingulate, the insula, the pre and postcentral gyri, and the angular gyrus.

Figures 9 and 10 are provided as an aid in interpreting the results and underlying GM and WM sites of concordance. In the GM, negative concordances are distributed among the frontal and dorsal parietal brain cortices. Positive concordances prevail in the occipital cortices and mixed results (positive and negative concordances) in the temporal and ventral parietal cortices. WM negative concordances are distributed in the superior corona radiata, cingulum, corpus callosum, cerebellar peduncle, thalamic radiation, and superior longitudinal fasciculus. Positive concordances are evidenced only in the posterior corona radiate. Mixed results are shown in the sagittal stratum. It is evident that while the more dorsal regions/tracts are predominantly characterized by decreases, the more we move toward ventral regions/tracts, the more we find positive or mixed results.

DISCUSSION

Although specific WM and GM abnormalities have already been described in ASD [Boddaert et al., 2004; Bonilha et al., 2008; Cauda et al., 2011; Ke et al., 2008, 2009; McAlonan et al., 2005, 2008], this work investigated the relationship between WM and GM abnormalities, using an innovative approach.

VBM and DTI data exhibit a convergence of results, as evidenced in the representational similarity analysis, and this allowed us to include the two data sets in a common ALE (see Fig. 1).

On the basis of the Hebbian hypothesis [Hebb, 1949], which describes a network of homogeneous functioning, we might expect to find concordance between WM-GM modifications, i.e., WM increases related to GM increases and vice-versa. Indeed, our results prevalently showed WM-GM concordances (positive or negative), and no GM

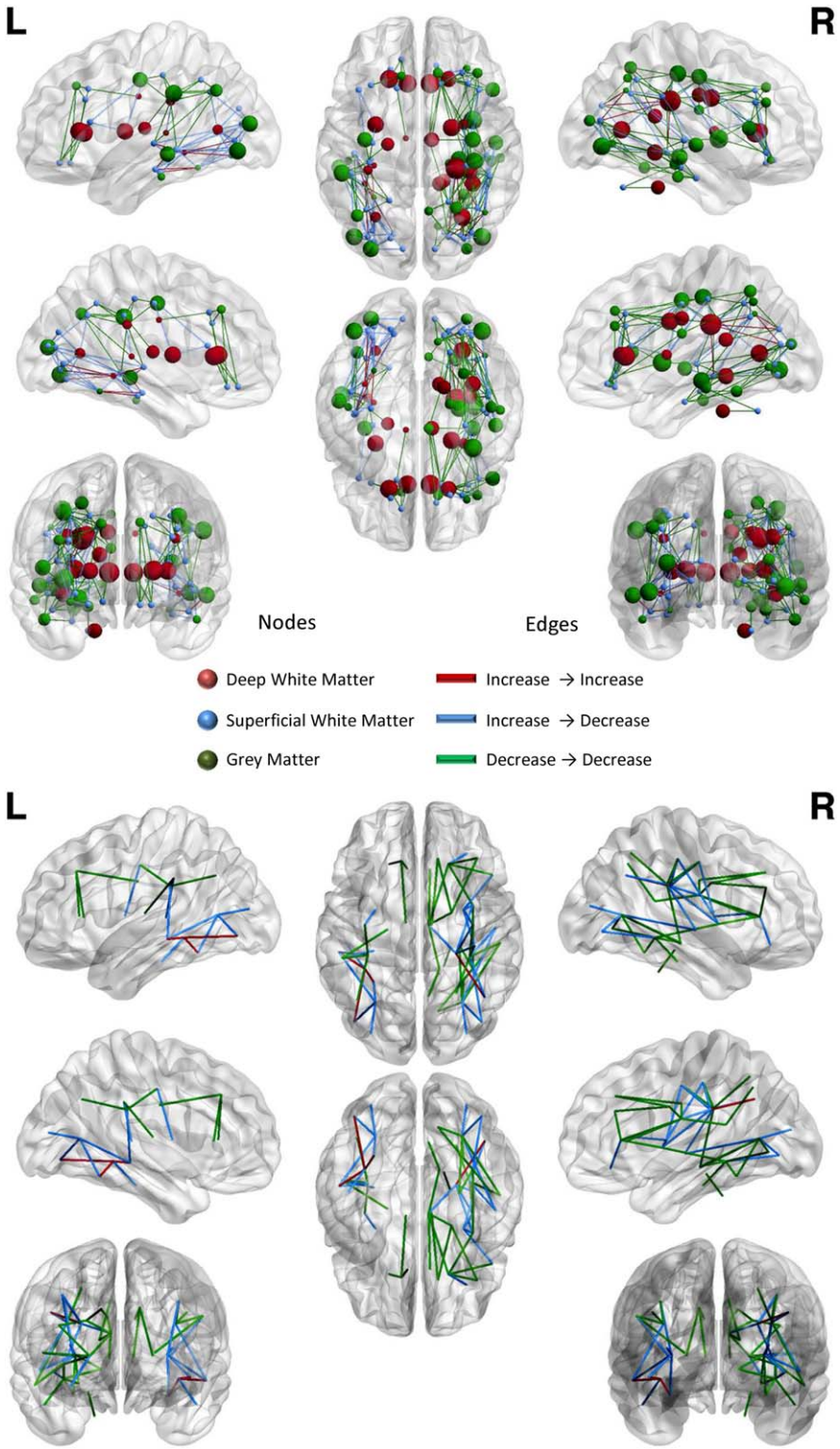

Figure 4.
(See legend on the following page.)

regions were uniquely identified for discordances, suggesting that GM abnormalities are always accompanied by WM alterations.

More in detail, we described three different types of relationships between WM and GM results: positive concordance, negative concordance, and discordance. Positive and negative concordances may refer to Gong's hypothesis [2012] of a trophic effect via direct axonal connections: positive concordances could be related to trophic effects, and negative concordances to hypotrophic effects. Discordance could represent an inhibitory role of WM on GM, a compensatory mechanism and/or a neurodevelopmental disorganization (increases in GM can be due to an increase in cell size, neural or glial cell genesis, spine density or even changes in blood flow or interstitial fluid).

We observed a consistent number of WM-GM concordances. In particular, we detected a few WM-GM increases, and several WM-GM decreases. It is possible that the concordance in decreases represents a network deficit involving WM-GM. Discordances were much less numerous and, interestingly, they resembled negative concordances (see Table IV) and were related to descendant fibers connecting the prefrontal or sensorimotor regions. In our opinion they could represent a mechanism for compensation.

We hypothesize that the contemporaneous presence of negative concordances and discordances in a certain brain region may be related to the contemporaneous presence of hypotrophic effects and compensatory mechanism and/or neurodevelopmental disorganization. To this aim, it is important to note that when we refer to a certain GM or WM region (such as for example in Figs. 8 and 9) the concordances/discordances attributed to that GM/WM region relate to connections between it and other different WM/GM regions. Thus one brain region may show contemporaneous concordances and discordances due to its different connections.

Indeed, according to our hypothesis the same (for example gray) region can show hypotrophic mechanisms in some WM regions and at the same time compensatory mechanisms in other WM regions, depending, for example, on the speed of the damage mechanism that may or may not leave time for a compensatory mechanism.

A disruption has been found in the balance of the brain network. In particular, an involvement of the frontoparietal regions and related fiber tracts, especially in the right hemisphere, has been detected. This could be related to a different right–left hemisphere vulnerability [Kelley, 2011; Raz et al., 1997]. Since different timing of hemispheric development has been described [Giedd et al., 1996; Thompson et al., 2000], a possible pathogenetic factor could damage the right hemisphere in the developmental step [Reiss et al., 1996] and this could be confirmed by the semantic and prosodic deficit clinically described in ASD [Braeutigam et al., 2008; McCleery et al., 2010; Radua et al., 2011]. Interestingly, the development of functional brain asymmetry between 1 and 3 years of age shows a right hemispheric predominance [Chiron et al., 1997].

Positive concordance (possible trophic mechanism) has been found in the left side; negative concordance (possible hypotrophic mechanism) and discordance (possible compensatory mechanism) are bilateral, but mainly in the right side [Dolcos et al., 2002; Giedd et al., 1996; Lapidot, 1987; Raz et al., 1997; Reiss et al., 1996].

The superior longitudinal fasciculus (SLF) exhibits bilateral negative concordance, strongly lateralized in the right hemisphere. The SLF has a broad neuroanatomic extent, connecting the frontal, parietal, and temporal lobes and may potentially have an important role in linking all the brain structures involved in social cognition. The anterior part of the superior longitudinal fasciculus (arcuate fasciculus) connects the perisylvian regions in the frontal, parietal and temporal lobes. In the left hemisphere, it connects the classical brain language regions. In the right hemisphere, it participates in visuospatial processing and other aspects of language, including affective prosody and semantics, core deficits in ASD [Braeutigam et al., 2008; McCleery et al., 2010; Radua et al., 2011]. Lesions to the right arcuate fasciculus impair understanding and production of modulation of pitch, intonation contours, melody, cadence, loudness, rhythm, stress, accent, and pauses. Prosody is used to transmit information above and beyond verbal-linguistic intent and to clarify the meaning of potentially ambiguous sentences by the judicious use of pauses and stresses, relating to the core deficit in quality communication skills in ASD [Grossman et al., 2010; McCann and Peppé, 2003; O'Connor, 2012]. In the right hemisphere, abnormalities of the SLF have implications in ASD due to its connection to the superior temporal sulcus (STS), a region known to be associated with processing biological motion [Jou et al., 2011a,b]. This region could also represent the anatomical correlate of some of the verbal

Figure 4.

Concordances between white matter and gray matter results. Upper panel: When a significant concordance is found between the results for a GM area and the corresponding WM fasciculus results it is represented by a straight line connecting the two areas. Node colors represent the areas: red, deep white matter; blue, superficial white matter; green, gray matter. Edge colors represent the type of concordance: red, increase→increase; blue decrease→decrease; green, increase→decrease. Lower panel: this image show the same dataset as the upper panel but here, to better visualize the concordances only the edges are represented: edge colors represent the type of concordance: red, increase→increase; blue decrease→decrease; green, increase→decrease. [Color figure can be viewed in the online issue, which is available at wileyonlinelibrary.com.]

TABLE III. Overview of concordant and discordant results

White matter	Grey matter	Type	Vol node A	Vol node B
Posterior corona radiata right	Angular gyrus	Increase–Increase	2,476	4,476
Sagittal stratum (include inferior longitudinal fasciculus and inferior fronto-occipital fasciculus) left	Fusiform gyrus	Increase–Increase	1,376	201
Sagittal stratum (include inferior longitudinal fasciculus and inferior fronto-occipital fasciculus) left	Inferior occipital gyrus	Increase–Increase	1,376	176
Sagittal stratum (include inferior longitidinal fasciculus and inferior fronto-occipital fasciculus) left	Middle temporal gyrus	Increase–Increase	1,376	6,601
Anterior corona radiata right	Lateral fronto-orbital gyrus	Increase–Decrease	12,526	12,526
External capsule left	Precentral gyrus	Increase–Decrease	9,651	12,526
External capsule right	Inferior frontal gyrus	Increase–Decrease	1,776	801
External capsule right	Insular	Increase–Decrease	1,776	6,676
External capsule right	Postcentral gyrus	Increase–Decrease	1,776	12,526
External capsule right	Precentral gyrus	Increase–Decrease	1,776	12,526
Posterior corona radiata right	Cingulate gyrus	Increase–Decrease	2,476	13,101
Posterior corona radiata right	Insular	Increase–Decrease	2,476	6,676
Posterior corona radiata right	Postcentral gyrus	Increase–Decrease	2,476	12,526
Posterior corona radiata right	Precentral gyrus	Increase–Decrease	2,476	12,526
Posterior thalamic radiation left	Fusiform gyrus	Increase–Decrease	1,376	201
Posterior thalamic radiation left	Inferior occipital gyrus	Increase–Decrease	1,376	176
Posterior thalamic radiation left	Middle occipital gyrus	Increase–Decrease	1,376	851
Posterior thalamic radiation left	Middle temporal gyrus	Increase–Decrease	1,376	6,601
Posterior thalamic radiation right	Inferior occipital gyrus	Increase–Decrease	1,376	451
Posterior thalamic radiation right	Middle occipital gyrus	Increase–Decrease	1,376	176
Posterior thalamic radiation right	Superior temporal gyrus	Increase–Decrease	1,376	4,476
Retrolenticular part of internal capsule left	Supramarginal gyrus	Increase–Decrease	12,526	501
Sagittal stratum (include inferior longitudinal fasciculus and inferior fronto-occipital fasciculus) left	Inferior temporal gyrus	Increase–Decrease	1,376	6,601
Sagittal stratum (include inferior longitidinal fasciculus and inferior fronto-occipital fasciculus) right	Inferior occipital gyrus	Increase–Decrease	9,651	451
SLF left	Middle temporal gyrus	Increase–Decrease	551	6,601
SLF right	Angular gyrus	Increase–Decrease	101	4,476
SLF right	Superior temporal gyrus	Increase–Decrease	101	4,476
Anterior corona radiata left	Superior frontal gyrus	Decrease–Decrease	12,526	1,001
Anterior corona radiata right	Cingulate gyrus	Decrease–Decrease	12,526	13,101
Anterior corona radiata right	Inferior frontal gyrus	Decrease–Decrease	12,526	801
Anterior corona radiata right	Insular	Decrease–Decrease	12,526	6,676
Anterior corona radiata right	Middle frontal gyrus	Decrease–Decrease	12,526	28,526
Cingulum left	Superior frontal gyrus	Decrease–Decrease	1,776	1,001
Cingulum right	Cingulate gyrus	Decrease–Decrease	1,051	13,101
Cingulum right	Superior frontal gyrus	Decrease–Decrease	1,051	101
Genu of corpus callosum left	Superior frontal gyrus	Decrease–Decrease	7,726	1,001
Genu of corpus callosum right	Cingulate gyrus	Decrease–Decrease	7,726	13,101
Middle cerebellar peduncle right	Parahippocampal gyrus	Decrease–Decrease	551	401
Posterior limb of internal capsule left	Supramarginal gyrus	Decrease–Decrease	1,201	501
Posterior thalamic radiation right	Fusiform gyrus	Decrease–Decrease	1,376	926
Posterior thalamic radiation right	Lingual gyrus	Decrease–Decrease	1,376	451
Posterior thalamic radiation right	Middle temporal gyrus	Decrease–Decrease	1,376	6,601
Sagittal stratum (include inferior longitidinal fasciculus and inferior fronto-occipital fasciculus) right	Fusiform gyrus	Decrease–Decrease	9,651	926

TABLE III. (continued).

White matter	Grey matter	Type	Vol node A	Vol node B
Sagittal stratum (include inferior longitidinal fasciculus and inferior fronto-occipital fasciculus) right	Hippocampus	Decrease–Decrease	9,651	251
Sagittal stratum (include inferior longitudinal fasciculus and inferior fronto-occipital fasciculus) right	Inferior temporal gyrus	Decrease–Decrease	9,651	1,401
Sagittal stratum (include inferior longitudinal fasciculus and inferior fronto-occipital fasciculus) right	Insular	Decrease–Decrease	9,651	6,676
Sagittal stratum (include inferior longitudinal fasciculus and inferior fronto-occipital fasciculus) right	Lingual gyrus	Decrease–Decrease	9,651	451
SLF left	Angular gyrus	Decrease–Decrease	551	3,651
SLF left	Precentral gyrus	Decrease–Decrease	551	12,526
SLF left	Supramarginal gyrus	Decrease–Decrease	551	501
SLF right	Middle temporal gyrus	Decrease–Decrease	101	6,601
SLF right	Postcentral gyrus	Decrease–Decrease	101	12,526
SLF right	Precentral gyrus	Decrease–Decrease	101	12,526
SLF right	Superior parietal lobule	Decrease–Decrease	101	2,476
Splenium of corpus callosum right	Cingulate gyrus	Decrease–Decrease	101	13,101
Splenium of corpus callosum right	Pre-cuneus	Decrease–Decrease	101	526
Superior corona radiata right	Cingulate gyrus	Decrease–Decrease	2,476	13,101
Superior corona radiata right	Middle frontal gyrus	Decrease–Decrease	2,476	28,526
Superior corona radiata right	Superior frontal gyrus	Decrease–Decrease	2,476	101

The columns "Vol Node A" indicate the dimension (expressed in mm^3) of the White Matter area that constitutes the node. The columns "Vol Node B" indicate the dimension (expressed in mm^3) of the Grey Matter area that constitutes the node.

and non-verbal communication impairments observed in ASD [Radua et al., 2011]. The STS multimodal regions are involved in cortical integration of both sensory and limbic information at the highest level, and are a key cortical region of the social brain, implicated in the social perceptual skills impaired in ASD [Boddaert et al., 2004]. The STS has also been found to be associated with disinhibition [Zamboni et al., 2008], a behavioral abnormality correlated with dysexecutive impairment in several diseases [Amanzio et al., 2011; Ball et al., 2010; Brocki and Bohlin, 2004]. Indeed, there are several studies documenting underconnectivity in executive functions in the fronto-parietal regions during tasks of planning and response inhibition in ASD [Just et al., 2007; Kana et al., 2007; Solomon et al., 2009].

Unlike the SLF, the sagittal stratum shows negative concordance in the right hemisphere but positive concordance in the left hemisphere. The sagittal stratum includes the inferior longitudinal fasciculus (ILF) and the inferior fronto-occipital fasciculus and connects the frontal, temporal, parietal, and occipital lobes. It has a role in integrating auditory and verbal inputs. The inferior fronto-occipital fasciculus plays an important role in linking all the components in what is commonly called the social brain [Jou et al., 2011a, b]. The right tract is severely affected and a potential mechanism for known impairments in facial emotion recognition in ASD has been suggested [Jou et al., 2011a,b]. The ILF connects the fusiform gyrus to the amygdale and hippocampus and plays an important role in social tasks requiring recognition of emotions from facial expressions [Pugliese et al., 2009].

With the impairment of the major pathways connecting the modules of the social brain (the inferior fronto-occipital fasciculus and the SLF), there is possible reliance on

TABLE IV. Univocal discordances

White matter	Grey matter	Vol node A	Vol node B
External capsule left	Precentral gyrus	9,651	12,526
External capsule right	Inferior frontal gyrus	1,776	801
External capsule right	Postcentral gyrus	1,776	12,526
External capsule right	Precentral gyrus	1,776	12,526
Retrolenticular part of internal capsule left	Supramarginal gyrus	12,526	501

TABLE V. Direction of the discordance

Grey matter	White matter	Type
Supramarginal gyrus	Retrolenticular part of internal capsule left	decrease–increase
Precentral gyrus	Posterior corona radiata right	decrease–increase
Postcentral gyrus	Posterior corona radiata right	decrease–increase
Cingulate gyrus	Posterior corona radiata right	decrease–increase
Insular	Posterior corona radiata right	decrease–increase
Inferior temporal gyrus	Sagittal stratum (include inferior longitudinal fasciculus and inferior fronto-occipital fasciculus) left	decrease–increase
Precentral gyrus	External capsule left	decrease–increase
Inferior frontal gyrus	External capsule right	decrease–increase
Precentral gyrus	External capsule right	decrease–increase
Postcentral gyrus	External capsule right	decrease–increase
Insular	External capsule right	decrease–increase
Lateral fronto-orbital gyrus	Anterior corona radiata right	Increase–decrease
Middle temporal gyrus	Posterior thalamic radiation (include optic radiation) left	Increase–decrease
Fusiform gyrus	Posterior thalamic radiation (include optic radiation) left	Increase–decrease
Middle occipital gyrus	Posterior thalamic radiation (include optic radiation) left	Increase–decrease
Inferior occipital gyrus	Posterior thalamic radiation (include optic radiation) left	Increase–decrease
Superior temporal gyrus	Posterior thalamic radiation (include optic radiation) right	Increase–decrease
Middle occipital gyrus	Posterior thalamic radiation (include optic radiation) right	Increase–decrease
Inferior occipital gyrus	Posterior thalamic radiation (include optic radiation) right	Increase–decrease
Inferior occipital gyrus	Sagittal stratum (include inferior longitidinal fasciculus and inferior fronto-occipital fasciculus) right	Increase–decrease
Middle temporal gyrus	Superior longitudinal fasciculus left	Increase–decrease
Angular gyrus	Superior longitudinal fasciculus right	Increase–decrease
Superior temporal gyrus	Superior longitudinal fasciculus right	Increase–decrease

smaller tracts resulting in inefficient cortico-cortical communication. The aberrations present in all fiber tracts exacerbate the problem. Deficits in long-range fiber tracts support the existence of reduced long-range connectivity. Whether social information processing is possible may depend on how severely impaired the main pathways are and whether alternative pathways are available.

Brain regions with higher betweenness centrality and the shortest path length are mainly related to the SLF and sagittal stratum connections, confirming the role of this longitudinal fasciculus in ASD. An analysis of the network evidenced, apart from the SLF and sagittal stratum, the precentral gyrus and the middle temporal gyrus in the left side, the insula, anterior cingulate cortex and precentral gyrus in the right side. This data is supported by network clustering, which revealed a relevant cluster with high connection density in the right side composed of the prefrontal, cingulate, insular, and sensorimotor regions. In the left side the same technique indicated a smaller cluster including the inferior occipital gyrus, fusiform gyrus, and middle temporal gyrus.

This right cluster evokes the previously described role of the prefrontal cortex and impaired abilities in ASD associated with the rostral prefrontal cortex. These concern multitasking, episodic memory, performance in novel situations, and mentalizing [Dumontheil et al., 2008].

The cingulate cortex has a well documented role in social cognition and has been found to be hypoactivated in patients with ASD while performing social tasks [Kennedy and Courchesne, 2008; Mundy, 2003]. Our results revealed a concordant decrease for the cingulate fibers. The posterior cingulate cortex is associated with self-referential processing, mentalizing, and development of theory of mind related to the anterior insula (linked to representing and/or monitoring the salience of one's own and others' emotions). The anterior cingulate cortex (pgACC) has a role in thinking about others' thoughts and beliefs, qualitatively impaired in ASD. PgACC-based networks may underlie autistic traits [Di Martino et al., 2009].

An anterior insula-based systems-level model has been proposed for investigating the critical interactions between multiple distinct brain systems in ASD. Network clustering evidenced an insular role especially among negative concordances in the right hemisphere. The anterior insula (AI) (considered part of the limbic integration cortex) is involved in interoceptive, affective, and empathic processes [Gu et al., 2013] and is part of a novelty detection or salience network integrating external sensory stimuli with internal states and has a relevant role in social processing networks [Anderson et al., 2011; Uddin and Menon, 2009]. The AI serves an integral function in representing and evaluating salient stimuli. It is uniquely positioned as a hub mediating interactions between large-scale brain networks involved in attentional and self-directed processes, and also mediates interactions between externally oriented attention and internally oriented cognitive processing. Dysfunctional AI

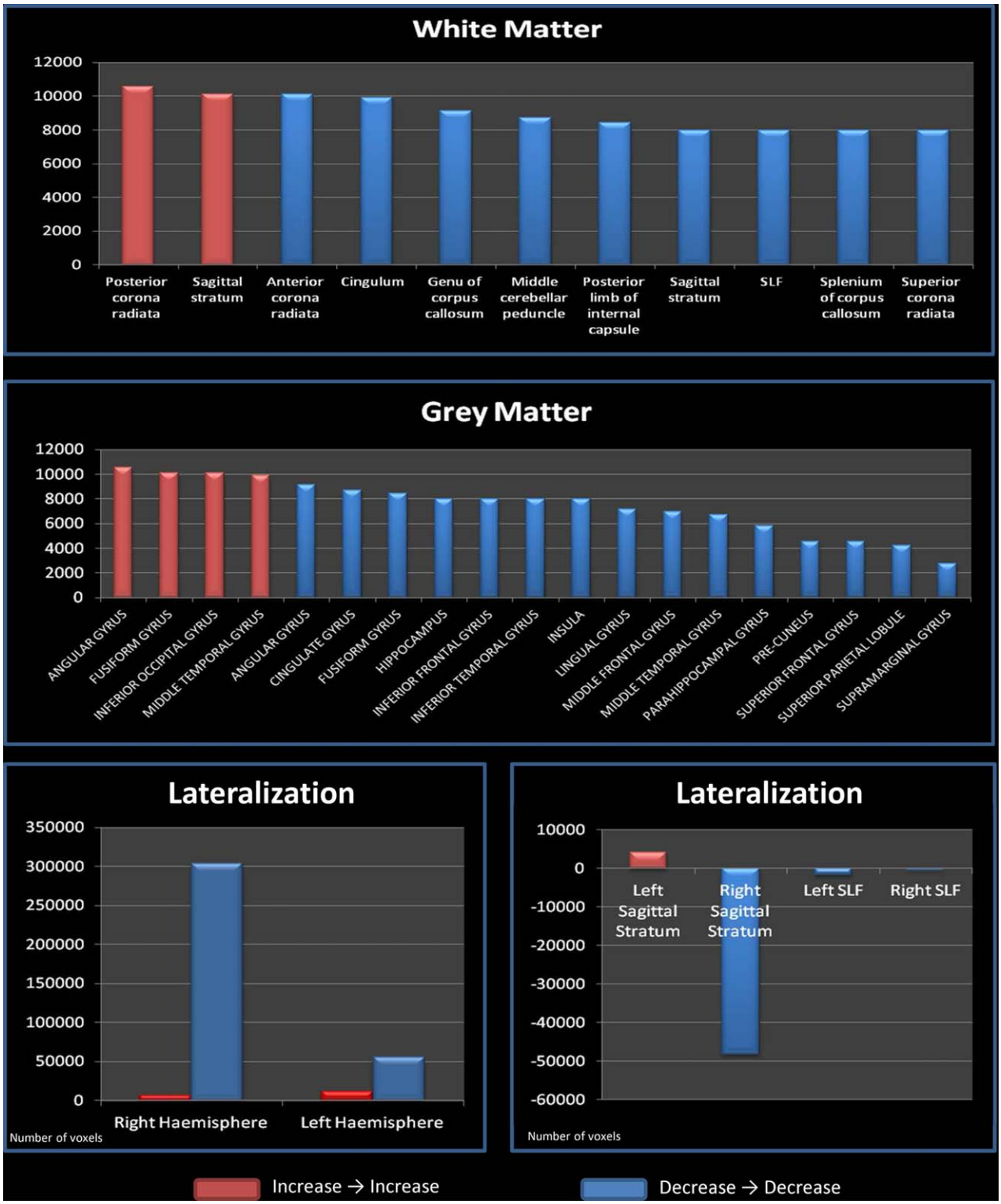
White Matter
12000
10000
8000
6000
4000
2000
0
Posterior corona radiata
Sagittal stratum
Anterior corona radiata
Cingulum
Genu of corpus callosum
Middle cerebellar peduncle
Posterior limb of internal capsule
Sagittal stratum
SLF
Splenium of corpus callosum
Superior corona radiata
Grey Matter
12000
10000
8000
6000
4000
2000
0
ANGULAR GYRUS
FUSIFORM GYRUS
INFERIOR OCCIPITAL GYRUS
MIDDLE TEMPORAL GYRUS
ANGULAR GYRUS
CINGULATE GYRUS
FUSIFORM GYRUS
HIPPOCAMPUS
INFERIOR FRONTAL GYRUS
INFERIOR TEMPORAL GYRUS
INSULA
LINGUAL GYRUS
MIDDLE FRONTAL GYRUS
MIDDLE TEMPORAL GYRUS
PARAHIPPOCAMPAL GYRUS
PRE-CUNEUS
SUPERIOR FRONTAL GYRUS
SUPERIOR PARIETAL LOBULE
SUPRAMARGINAL GYRUS
Lateralization
350000
300000
250000
200000
150000
100000
50000
0
Right Haemisphere
Left Haemisphere
Number of voxels
Lateralization
10000
0
-10000
-20000
-30000
-40000
-50000
-60000
Left Sagittal Stratum
Right Sagittal Stratum
Left SLF
Right SLF
Number of voxels
Increase → Increase
Decrease → Decrease

Figure 5.

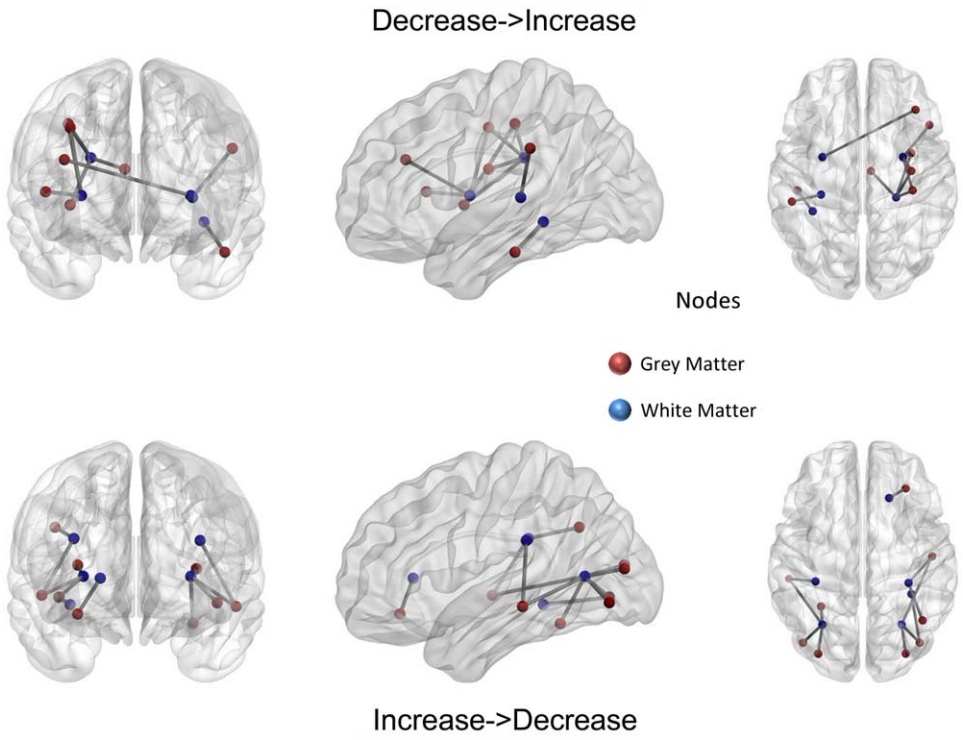

Figure 6.

Discordances between white matter and gray matter results. When a significant discordance is found between the results for a GM area and the corresponding WM fasciculus results it is represented by a straight line connecting the two areas. Node colors represent the areas: red, gray matter; blue, white matter. [Color figure can be viewed in the online issue, which is available at wileyonlinelibrary.com.]

connectivity could play an important role in ASD, resulting in an impaired drive to identify the emotions and thoughts of others and to respond with an appropriate emotion [Kosaka et al., 2010; Uddin and Menon, 2009].

The presence of von Economo neurons (VENs) in the frontoinsular cortex (FI) has been linked to a possible role in the integration of bodily feelings, emotional regulation, goal-directed behaviors, and in fast intuitive evaluation of complex social situations [Allman et al., 2011; Cauda et al., 2012]. A higher ratio of VENs to pyramidal neurons than control subjects has been detected and this result may reflect the presence of neuronal overgrowth and may also be related to alterations in migration, cortical lamination, and apoptosis in ASD [Cauda et al., 2012; Santos et al., 2011].

The left network cluster is related to the inferior occipital gyrus, fusiform gyrus, and middle temporal gyrus. The posterior middle temporal gyrus (pMTG) has a role in processing semantic extralinguistic inputs also related to the context and is connected to the left inferior frontal gyrus that links pMTG data to recalled information from other regions. This deficit closely reflects the semantic deficit in social skills in ASD. The fusiform gyrus has been found to be involved in facial processing tasks in ASD

Figure 5.

Gray matter and white matter distributions. Upper panel: Deep WM areas where a positive (increase→increase) or a negative (decrease→decrease) concordance is found. Middle panel: GM areas where a positive (increase→increase) or a negative (decrease→decrease) concordance is found. Lower panel: Concordance lateralization. Left: global lateralization, the *y* axis shows the total number of voxels present in areas that showed a positive (red color) or negative (blue color) concordance; Right: sagittal stratum and superior longitudinal fasciculum lateralization, the *y* axis shows the total number of voxels present in areas that showed a positive (red color) or negative (blue color) concordance. To further differentiate positive and negative concordances the first are represented on the *y* axis with positive numbers and the second with negative numbers. [Color figure can be viewed in the online issue, which is available at wileyonlinelibrary.com.]

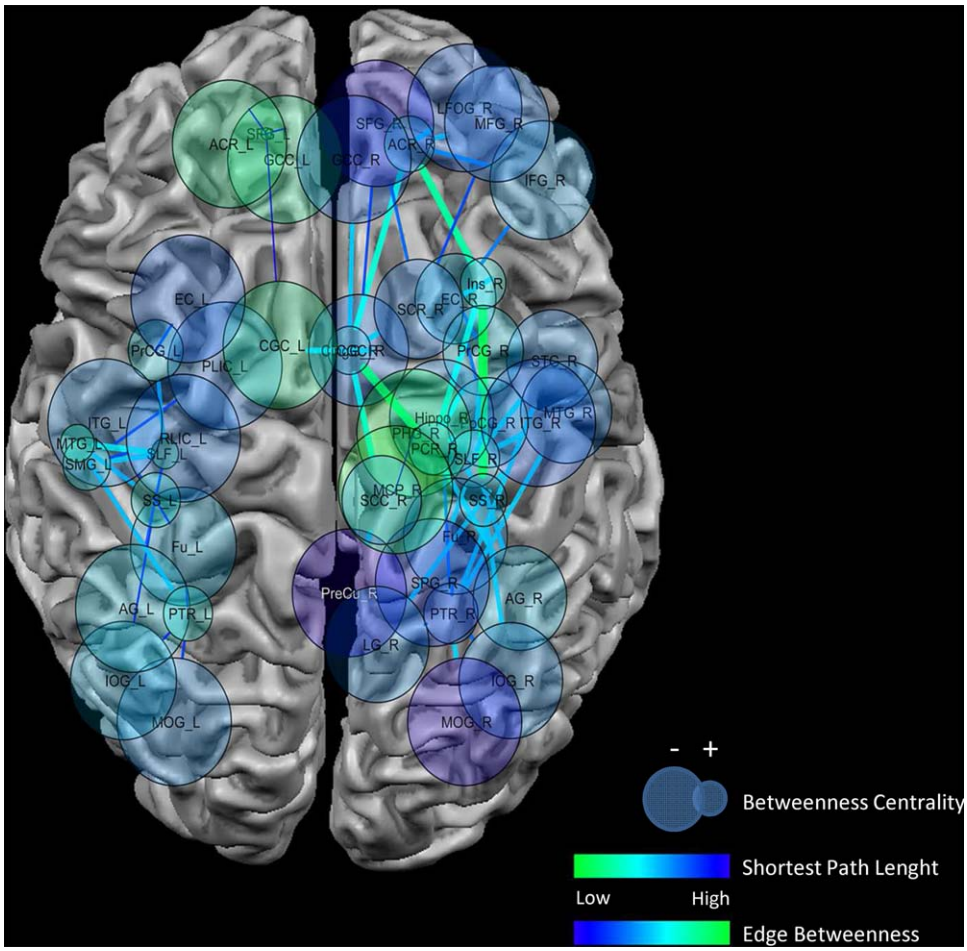

Figure 7.

Topological analysis of the results. Upper panel: the graph shows a different view of THE nodes and edges represented in Figure 4. This image shows a series of topological measures of the network constituted by significant concordances. Node dimension indicates betweenness centrality (smaller nodes = higher betweenness centrality); node color indicates the average shortest path length (green to blue = lower to higher values); Edge color and dimension indicates the edge betweenness (blue to green = lower to higher values). [Color figure can be viewed in the online issue, which is available at wileyonlinelibrary.com.]

[Anderson et al., 2011; Kleinhans et al., 2008, Koshino et al., 2008].

We also found negative concordance in the bilateral precentral gyrus, left supramarginal gyrus, right inferior frontal gyrus, and bilateral superior frontal gyrus. Intriguingly, these regions are involved in the mirror neuron system. GM thinning in autism in regions associated with the mirror-neuron system (inferior parietal lobule, premotor cortex, mostly its ventral part, plus the caudal part of the inferior frontal gyrus roughly corresponding to the pars opercularis of Broca's area) were correlated with social and communication deficits [Cattaneo and Rizzolatti, 2009; Keller et al., 2011; Kilner et al., 2007; Rizzolatti and Craighero, 2004].

The right temporo-parietal junction has been indicated as having a role in mentalizing and in mindblindness (deficit in representing mental states) in ASD [Lombardo et al., 2011] but other authors have expressed the need for caution in accepting a crucial role of the right temporo-parietal junction in intention understanding because this region is also activated in tasks involving attention [Rizzolatti and Fabbri-Destro, 2010].

The corpus callosum (CC) is characterized by negative concordance, especially in the genu and splenium, supporting the hypothesis of impaired inter-hemispheric communication, particularly involving the frontal and parietal regions. The CC plays an integral role in relaying sensory, motor, and cognitive information from homologous regions in the two hemispheres. A significant difference in the anterior-most part and anterior body of the CC between ASD patients and controls has been described [He et al., 2010] and many young people with callosal agenesis show theory of mind and

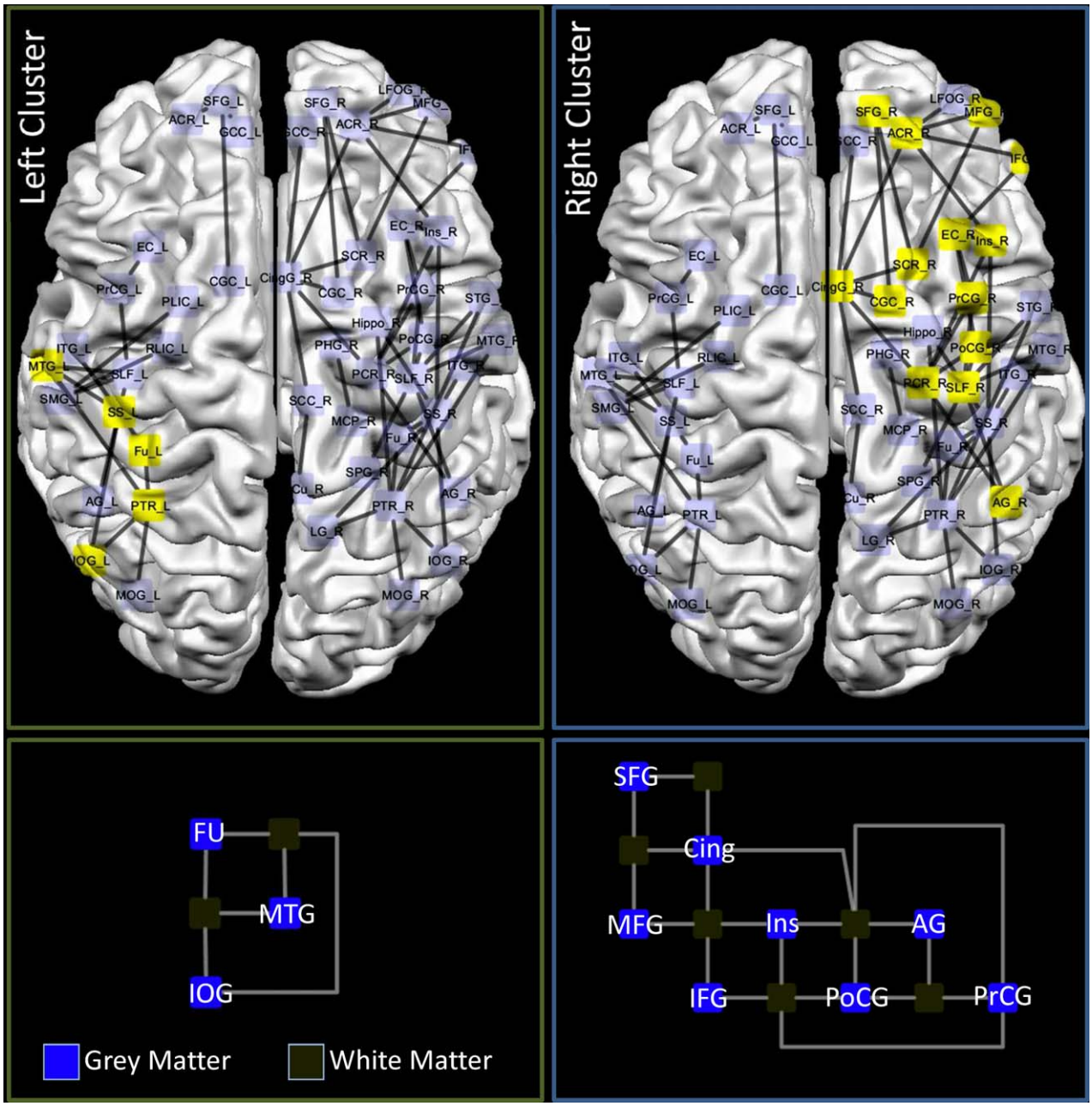

Figure 8.

Network clusterization. Upper panel: the yellow nodes and edges represent the results of a K-core clustering of the concordance results. Indeed the clustering algorithm reported two clusters in our data: one right with 14 nodes and one in the left hemisphere with 5 nodes. Lower panel: orthogonal representation of the left and right clusters. [Color figure can be viewed in the online issue, which is available at wileyonlinelibrary.com.]

emotion-processing deficits akin to those seen in autism [Booth et al., 2011].

Negative concordances were also found in the posterior thalamic radiation. This points to a thalamic involvement in ASD. Reduced GM density in the thalamus, right cerebellum hemisphere and left temporo-parietal cortex correlates with intellectual disabilities in ASD [Spencer et al., 2006]. Recent findings support evidence implicating disturbances in the thalamo-frontal connections in autism and highlight the role of

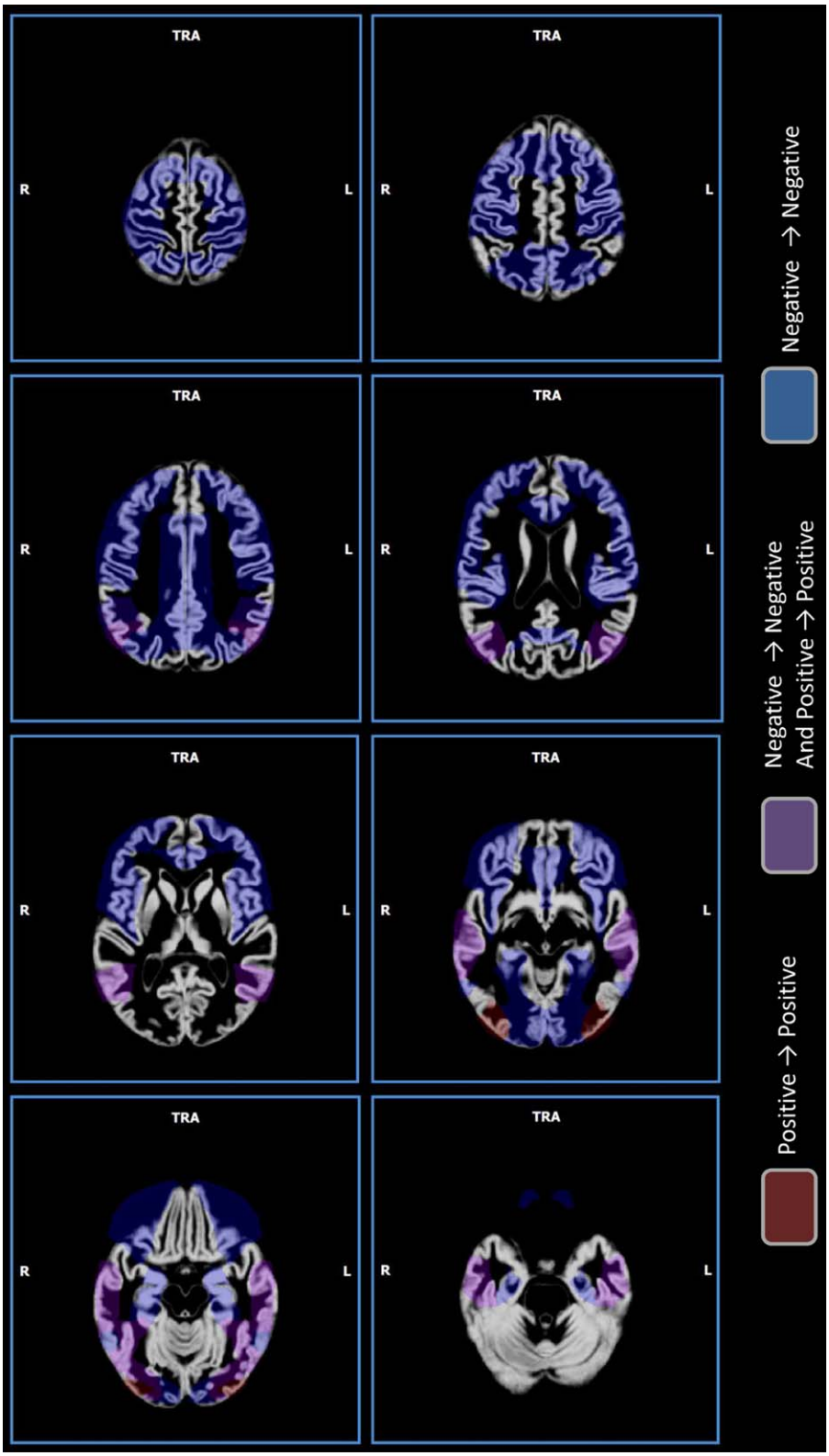

Figure 9.

Gray matter sites of concordance. Sites of concordance. Red indicates positive concordances (increase→increase); blue indicates negative concordances (decrease→decrease); violet indicates areas where a mix of positive concordances and negative concordances was found. [Color figure can be viewed in the online issue, which is available at wileyonlinelibrary.com.]

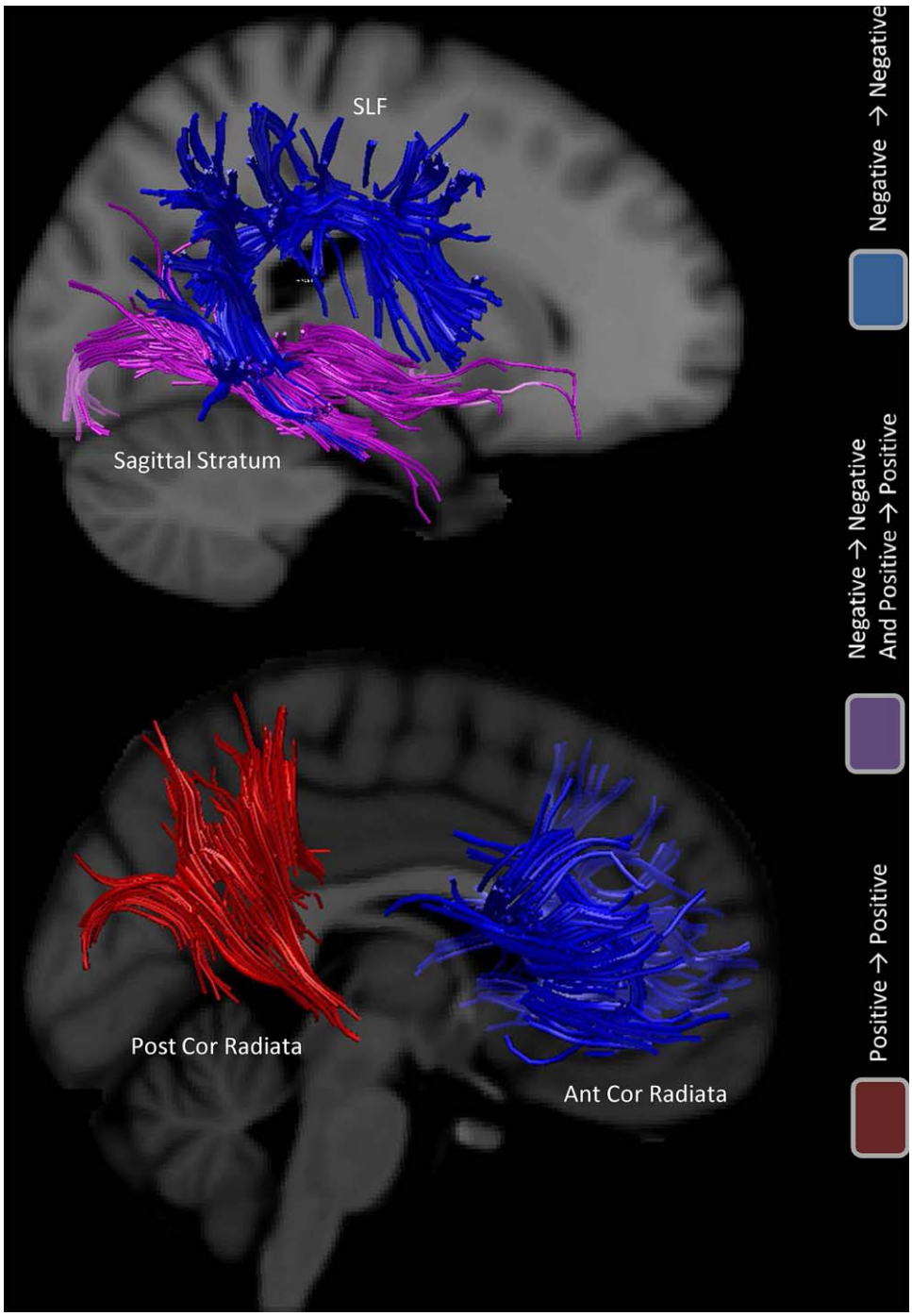

Figure 10.
White matter principal sites of concordance. Sites of concordance. Red indicates positive concordances (increase→increase); blue indicates negative concordances (decrease→decrease); violet indicates areas where a mix of positive concordances and negative concordances was found. [Color figure can be viewed in the online issue, which is available at wileyonlinelibrary.com.]

hypoconnectivity between the frontal cortex and thalamus in ASD [Cheon et al., 2011].

Concordance has not only been detected for longitudinal tracts but also for dorso-ventral tracts, such as the corona radiata, connecting the frontal, parietal and insular regions with the basal ganglia. These fibers, not only involved in motor circuits but also show negative concordance or discordance. The fronto-striatal regions differ in structure, metabolism, and functionality in ASD compared to those of healthy individuals. The fronto and striatal brain regions (such as the head of the caudate nucleus, superior frontal gyrus BA11, anterior cingulate, dorsolateral prefrontal cortex) are reciprocally connected to each other and the thalamus and are involved not only in ASD [Haznedar et al., 2006; Polšek et al., 2011] but also interestingly in disorders clinically related to differential diagnosis of ASD such as obsessive compulsive disorder [Gonçalves et al., 2011; van den Heuvel et al., 2011] and schizophrenia [Andreasen et al., 1994; Robbins, 1990; van Haren et al., 2007]. Abnormalities of these regions in ASD have been related to motor abnormalities (abnormal gait sequencing, delayed walking development, abnormal hand positioning), impaired sensory-motor gating, repetitive, and stereotyped behavior. Caudate nucleus volume correlates with repetitive and stereotyped behavior and social-communication ADI-R total score [Rojas et al., 2006].

Middle peduncular cerebellar fibers have negative concordances. The cerebellum is involved in ASD and is intrinsically connected with itself as well as with the cerebral cortex via the thalamus; it receives afferents from the prefrontal cortex (BA4-primary motor cortex, BA6-premotor cortex), involved in ASD. The deficit network includes the temporo-parietal regions (BA40) and the superior parietal lobe (BA7), which have been linked to mentalizing deficits in Asperger's syndrome [Ecker et al., 2010].

These findings suggest that ASD is unlikely to be associated with abnormality in one particular location alone. Instead ASD reflects abnormalities within a particular neural system or multiple systems that could be partly different in distinct clinical phenotypes [Anderson et al., 2011].

WM maturation reshapes structural connectivity with major structural modules and hubs in place by 2 years of age but also continuing in the late development of the human brain (2–18 yrs of age). These WM changes likely play a significant role in establishing interregional processing and neuronal synchrony in the brain [Hagmann et al., 2010]. The role of systemic inflammation in disrupting the developmental program of white matter has been investigated [Favrais et al., 2011] and clinical data on altered inflammation in ASD were recently published [Schwartz and Shechter, 2010]. The prenatal role of endocrinological input, especially sex hormones such as testosterone, is also involved in early organization of the brain [Baron-Cohen et al., 2011].

In conclusion, we have shown that there is a statistically significant topological concordance between the results of GM and WM studies in ASD. Negative concordances are bilateral but with a higher prevalence in the right hemisphere. Positive concordances are in the left hemisphere. Discordance reflects the spatial distribution of negative concordances.

These results represent a new step in focusing on the biological basis of the core symptoms of ASD that we have described as an altered network balance, with a different hemispheric representation, interestingly possibly related to different timing of hemispheric development. A pathogenetic factor activating a genetic input could alter the balance of brain development, also involving epigenetics, possibly mediated by an inflammatory and endocrinological mechanism and widely disrupting brain connectivity, thus reflecting the pervasive symptoms dramatically damaging quality communication and social skills in the early development of ASD patients.

REFERENCES

American Psychiatric Association (APA) (2000): Diagnostic and Statistical Manual of Mental Disorders, Fourth Edition, Text Revision (DSM-IV-TR®).

Allman JM, Tetreault NA, Hakeem AY, Manaye KF, Semendeferi K, Erwin JM, Park S, Goubert V, Hof PR (2011): The von economo neurons in the frontoinsular and anterior cingulate cortex. Ann N Y Acad Sci 1225:59–71.

Alvarez-Hamelina I, Dall'Astaa L, Barrata A, Vespignani A (2006): K-Core decomposition: A tool for the visualization of large scale networks. Advances in Neural Information Processing Systems 18, 41. arXiv:cs/0504107 [cs.NI].

Amanzio M, Benedetti F, Porro CA, Palermo S, Cauda F (2013): Activation likelihood estimation meta-analysis of brain correlates of placebo analgesia in human experimental pain. Hum Brain Mapp 34:738–752.

Amanzio M, Torta DM, Sacco K, Cauda F, D'Agata F, Duca S, Leotta D, Palermo S, Geminiani GC (2011): Unawareness of deficits in Alzheimer's disease: Role of the cingulate cortex. Brain 134:1061–1076.

Anagnostou E, Taylor MJ (2011): Review of neuroimaging in autism spectrum disorders: What have we learned and where we go from here. Mol Autism 2:4.

Anderson JS, Nielsen JA, Froehlich AL, DuBray MB, Druzgal TJ, Cariello AN, Cooperrider JR, Zielinski BA, Ravichandran C, Fletcher PT, Alexander AL, Bigler ED, Lange N, Lainhart JE (2011): Functional connectivity magnetic resonance imaging classification of autism. Brain 134 (Part 12):3742–3754.

Andreasen NC, Flashman L, Flaum M, Arndt S, Swayze V, O'Leary DS, Ehrhardt JC, Yuh WT (1994): Regional brain abnormalities in schizophrenia measured with magnetic resonance imaging. JAMA 272:1763–1769.

Ashburner J, Friston KJ (2000): Voxel-based morphometry—The methods. Neuroimage 11:805–821.

Bader GD, Hogue CW (2003): An automated method for finding molecular complexes in large protein interaction networks. BMC Bioinformatics 4:2.

Ball SL, Holland AJ, Watson PC, Huppert FA (2010): Theoretical exploration of the neural bases of behavioural disinhibition, apathy and executive dysfunction in preclinical Alzheimer's disease in people with Down's syndrome: Potential involvement of multiple frontal-subcortical neuronal circuits. J Intellect Disabil Res 54:320–336.

Barnea-Goraly N, Kwon H, Menon V, Eliez S, Lotspeich L, Reiss AL (2004): White matter structure in autism: Preliminary evidence from diffusion tensor imaging. Biol Psychiatry 55:323–326.

Baron-Cohen S, Lombardo MV, Auyeung B, Ashwin E, Chakrabarti B, Knickmeyer R (2011): Why are autism spectrum conditions more prevalent in males? PloS Biol 9:e1001081.

Boddaert N, Chabane N, Gervais H, Good CD, Bourgeois M, Plumet MH, Barthélémy C, Mouren MC, Artiges E, Samson Y, Brunelle F, Frackowiak RS, Zilbovicius M (2004): Superior temporal sulcus anatomical abnormalities in childhood autism: A voxel-based morphometry MRI study. Neuroimage 23:364–369.

Bonilha L, Cendes F, Rorden C, Eckert M, Dalgalarrondo P, Li LM, Steiner CE (2008): Gray and white matter imbalance—Typical structural abnormality underlying classic autism? Brain Dev 30:396–401.

Booth R, Wallace GL, Happé F (2011): Connectivity and the corpus callosum in autism spectrum conditions: insights from comparison of autism and callosal agenesis. Prog Brain Res 189:303–317.

Braeutigam S, Swithenby SJ, Bailey AJ (2008): Contextual integration the unusual way: A magnetoencephalographic study of responses to semantic violation in individuals with autism spectrum disorders. Eur J Neurosci 27:1026–1036.

Brocki KC, Bohlin G (2004): Executive functions in children aged 6 to 13: A dimensional and developmental study. Dev Neuropsychol 26:571–593.

Calderoni S, Retico A, Biagi L, Tancredi R, Muratori F, Tosetti M (2012): Female children with autism spectrum disorder: An insight from mass-univariate and pattern classification analyses. Neuroimage 59:1013–1022.

Cattaneo L, Rizzolatti G (2009): The mirror neuron system. Arch Neurol 66:557–560.

Cauda F, Geda E, Sacco K, D'Agata F, Duca S, Geminiani G, Keller R (2011): Grey matter abnormality in autism spectrum disorder: An activation likelihood estimation meta-analysis study. J Neurol Neurosurg Psychiatry 82:1304–1313.

Cauda F, Torta DM, Sacco K, D'Agata F, Geda E, Duca S, Geminiani G, Vercelli A (2012): Functional anatomy of cortical areas characterized by Von Economo neurons. Brain Struct Funct 218:1–20.

Cheng Y, Chou KH, Chen IY, Fan YT, Decety J, Lin CP (2010): Atypical development of white matter microstructure in adolescents with autism spectrum disorders. Neuroimage 50:873–882.

Cheon KA, Kim YS, Oh SH, Park SY, Yoon HW, Herrington J, Nair A, Koh YJ, Jang DP, Kim YB, Leventhal BL, Cho ZH, Castellanos FX, Schultz RT (2011): Involvement of the anterior thalamic radiation in boys with high functioning autism spectrum disorders: a Diffusion Tensor Imaging study. Brain Res 1417:77–86.

Cheung C, Chua SE, Cheung V, Khong PL, Tai KS, Wong TK, Ho TP, McAlonan GM (2009): White matter fractional anisotrophy differences and correlates of diagnostic symptoms in autism. J Child Psychol Psychiatry 50:1102–1112.

Chiron C, Jambaque I, Nabbout R, Lounes R, Syrota A, Dulac O (1997): The right brain hemisphere is dominant in human infants. Brain 120 (Part 6):1057–1065.

Chua SE, Cheung C, Cheung V, Tsang JT, Chen EY, Wong JC, Cheung JP, Yip L, Tai KS, Suckling J, McAlonan GM (2007): Cerebral grey, white matter and csf in never-medicated, first-episode schizophrenia. Schizophr Res 89:12–21.

Craig MC, Zaman SH, Daly EM, Cutter WJ, Robertson DM, Hallahan B, Toal F, Reed S, Ambikapathy A, Brammer M, Murphy CM, Murphy DG (2007): Women with autistic-spectrum disorder: Magnetic resonance imaging study of brain anatomy. Br J Psychiatry 191:224–228.

Curk T, Demsar J, Xu Q, Leban G, Petrovic U, Bratko I, Shaulsky G, Zupan B (2005): Microarray data mining with visual programming. Bioinformatics 21:396–398.

Di Martino A, Ross K, Uddin LQ, Sklar AB, Castellanos FX, Milham MP (2009): Functional brain correlates of social and nonsocial processes in autism spectrum disorders: An activation likelihood estimation meta-analysis. Biol Psychiatry 65:63–74.

Dolcos F, Rice HJ, Cabeza R (2002): Hemispheric asymmetry and aging: right hemisphere decline or asymmetry reduction. Neurosci Biobehav Rev 26:819–825.

Douaud G, Smith S, Jenkinson M, Behrens T, Johansen-Berg H, Vickers J, James S, Voets N, Watkins K, Matthews PM, James A (2007): Anatomically related grey and white matter abnormalities in adolescent-onset schizophrenia. Brain 130:2375–2386.

Dumontheil I, Burgess PW, Blakemore SJ (2008): Development of rostral prefrontal cortex and cognitive and behavioural disorders. Dev Med Child Neurol 50:168–181.

Ecker C, Rocha-Rego V, Johnston P, Mourao-Miranda J, Marquand A, Daly EM, Brammer MJ, Murphy C, Murphy DG, Consortium MA (2010): Investigating the predictive value of whole-brain structural MR scans in autism: A pattern classification approach. Neuroimage 49:44–56.

Eickhoff SB, Bzdok D, Laird AR, Kurth F, Fox PT (2012): Activation likelihood estimation meta-analysis revisited. Neuroimage 59:2349–2361.

Eickhoff SB, Laird AR, Grefkes C, Wang LE, Zilles K, Fox PT (2009): Coordinate-based activation likelihood estimation meta-analysis of neuroimaging data: A random-effects approach based on empirical estimates of spatial uncertainty. Hum Brain Mapp 30:2907–2926.

Favrais G, van de Looij Y, Fleiss B, Ramanantsoa N, Bonnin P, Stoltenburg-Didinger G, Lacaud A, Saliba E, Dammann O, Gallego J, Sizonenko S, Hagberg H, Leliűvre V, Gressens P (2011): Systemic inflammation disrupts the developmental program of white matter. Ann Neurol 70:550–565.

Giedd JN, Snell JW, Lange N, Rajapakse JC, Casey BJ, Kozuch PL, Vaituzis AC, Vauss YC, Hamburger SD, Kaysen D, Rapoport JL (1996): Quantitative magnetic resonance imaging of human brain development: ages 4-18. Cereb Cortex 6:551–560.

Gong G, He Y, Chen ZJ, Evans AC (2012): Convergence and divergence of thickness correlations with diffusion connections across the human cerebral cortex. Neuroimage 59:1239–1248.

Gonçalves Ó, Carvalho S, Leite J, Pocinho F, Relvas J, Fregni F (2011): Obsessive compulsive disorder as a functional interhemispheric imbalance at the thalamic level. Med Hypotheses 77:445–447.

Grossman RB, Bemis RH, Plesa Skwerer D, Tager-Flusberg H (2010): Lexical and affective prosody in children with high-functioning autism. J Speech Lang Hear Res 53:778–793.

Gu X, Liu X, Van Dam NT, Hof PR, Fan J (2013): Cognition-Emotion Integration in the Anterior Insular Cortex. Cereb Cortex 23:20–27.

Hagmann P, Sporns O, Madan N, Cammoun L, Pienaar R, Wedeen VJ, Meuli R, Thiran JP, Grant PE (2010): White matter maturation reshapes structural connectivity in the late developing human brain. Proc Natl Acad Sci USA 107:19067–19072.

Haznedar MM, Buchsbaum MS, Hazlett EA, LiCalzi EM, Cartwright C, Hollander E (2006): Volumetric analysis and three-

dimensional glucose metabolic mapping of the striatum and thalamus in patients with autism spectrum disorders. Am J Psychiatry 163:1252–1263.

He Y, Chen Z, Evans A (2008): Structural insights into aberrant topological patterns of large-scale cortical networks in Alzheimer's disease. J Neurosci 28:4756–4766.

He Y, Dagher A, Chen Z, Charil A, Zijdenbos A, Worsley K, Evans A (2009): Impaired small-world efficiency in structural cortical networks in multiple sclerosis associated with white matter lesion load. Brain 132 (Part 12):3366–3379.

He Q, Duan Y, Karsch K, Miles J (2010): Detecting corpus callosum abnormalities in autism based on anatomical landmarks. Psychiatry Res 183:126–132.

Hebb DO (1949): The Organization of Behavior. New York: Wiley.

Hua K, Oishi K, Zhang J, Wakana S, Yoshioka T, Zhang W, Akhter KD, Li X, Huang H, Jiang H, van Zijl P, Mori S (2009): Mapping of functional areas in the human cortex based on connectivity through association fibers. Cereb Cortex 19:1889–1895.

Hyde KL, Samson F, Evans AC, Mottron L (2010): Neuroanatomical differences in brain areas implicated in perceptual and other core features of autism revealed by cortical thickness analysis and voxel-based morphometry. Hum Brain Mapp 31:556–566.

Jou RJ, Jackowski AP, Papademetris X, Rajeevan N, Staib LH, Volkmar FR (2011a): Diffusion tensor imaging in autism spectrum disorders: Preliminary evidence of abnormal neural connectivity. Aust N Z J Psychiatry 45:153–162.

Jou RJ, Mateljevic N, Kaiser MD, Sugrue DR, Volkmar FR, Pelphrey KA (2011b): Structural neural phenotype of autism: preliminary evidence from a diffusion tensor imaging study using tract-based spatial statistics. AJNR Am J Neuroradiol 32:1607–1613.

Just MA, Cherkassky VL, Keller TA, Kana RK, Minshew NJ (2007): Functional and anatomical cortical underconnectivity in autism: Evidence from an FMRI study of an executive function task and corpus callosum morphometry. Cereb Cortex 17:951–961.

Kana RK, Keller TA, Minshew NJ, Just MA (2007): Inhibitory control in high-functioning autism: Decreased activation and underconnectivity in inhibition networks. Biol Psychiatry 62:198–206.

Ke X, Hong S, Tang T, Zou B, Li H, Hang Y, Zhou Z, Ruan Z, Lu Z, Tao G, Liu Y (2008): Voxel-based morphometry study on brain structure in children with high-functioning autism. Neuroreport 19:921–925.

Ke X, Tang T, Hong S, Hang Y, Zou B, Li H, Zhou Z, Ruan Z, Lu Z, Tao G, Liu Y (2009): White matter impairments in autism, evidence from voxel-based morphometry and diffusion tensor imaging. Brain Res 1265:171–177.

Keller TA, Kana RK, Just MA (2007): A developmental study of the structural integrity of white matter in autism. Neuroreport 18:23–27.

Keller R, Bugiani S, Fantin P, Pirfo E (2011): Mirror neurons and autism. Giorn Ital Psicopatol 17:404–412.

Kelley MP (2011): Schizotypy and hemisphericity. Psychol Rep 109:533–552.

Kennedy DP, Courchesne E (2008): Functional abnormalities of the default network during self- and other-reflection in autism. Soc Cogn Affect Neurosci 3:177–190.

Kilner JM, Friston KJ, Frith CD (2007): The mirror-neuron system: A Bayesian perspective. Neuroreport 18:619–623.

Kleinhans NM, Richards T, Sterling L, Stegbauer KC, Mahurin R, Johnson LC, Greenson J, Dawson G, Aylward E (2008): Abnormal functional connectivity in autism spectrum disorders during face processing. Brain 131 (Part 4):1000–1012.

Kosaka H, Omori M, Munesue T, Ishitobi M, Matsumura Y, Takahashi T, Narita K, Murata T, Saito DN, Uchiyama H, Morita T, Kikuchi M, Mizukami K, Okazawa H, Sadato N, Wada Y (2010): Smaller insula and inferior frontal volumes in young adults with pervasive developmental disorders. Neuroimage 50:1357–1363.

Koshino H, Kana RK, Keller TA, Cherkassky VL, Minshew NJ, Just MA (2008): fMRI investigation of working memory for faces in autism: Visual coding and underconnectivity with frontal areas. Cereb Cortex 18:289–300.

Kriegeskorte N, Mur M, Bandettini P (2008): Representational similarity analysis—Connecting the branches of systems neuroscience. Front Syst Neurosci 2:4.

Laird AR, Fox PM, Price CJ, Glahn DC, Uecker AM, Lancaster JL, Turkeltaub PE, Kochunov P, Fox PT (2005): ALE meta-analysis: controlling the false discovery rate and performing statistical contrasts. Hum Brain Mapp 25:155–164.

Lancaster JL, Woldorff MG, Parsons LM, Liotti M, Freitas CS, Rainey L, Kochunov PV, Nickerson D, Mikiten SA, Fox PT (2000): Automated talairach atlas labels for functional brain mapping. Hum Brain Mapp 10:120–131.

Lancaster JL, Tordesillas-Gutiérrez D, Martinez M, Salinas F, Evans A, Zilles K, Mazziotta JC, Fox PT (2007): Bias between MNI and Talairach coordinates analyzed using the ICBM-152 brain template. Hum Brain Mapp 28:1194–1205.

Lapidot MB (1987): Does the brain age uniformly? Evidence from effects of smooth pursuit eye movements on verbal and visual tasks. J Gerontol 42:329–331.

Le Bihan D, Mangin JF, Poupon C, Clark CA, Pappata S, Molko N, Chabriat H (2001): Diffusion tensor imaging: Concepts and applications. J Magn Reson Imaging 13:534–546.

Lerch JP, Worsley K, Shaw WP, Greenstein DK, Lenroot RK, Giedd J, Evans AC (2006): Mapping anatomical correlations across cerebral cortex (MACACC) using cortical thickness from MRI. Neuroimage 31:993–1003.

Lombardo MV, Chakrabarti B, Bullmore ET, Baron-Cohen S, Consortium MA (2011): Specialization of right temporo-parietal junction for mentalizing and its relation to social impairments in autism. Neuroimage 56:1832–1838.

McAlonan GM, Daly E, Kumari V, Critchley HD, van Amelsvoort T, Suckling J, Simmons A, Sigmundsson T, Greenwood K, Russell A, Schmitz N, Happe F, Howlin P, Murphy DG (2002): Brain anatomy and sensorimotor gating in Asperger's syndrome. Brain 125 (Part 7):1594–606.

McAlonan GM, Cheung V, Cheung C, Suckling J, Lam GY, Tai KS, Yip L, Murphy DG, Chua SE (2005): Mapping the brain in autism. A voxel-based MRI study of volumetric differences and intercorrelations in autism. Brain 128 (Part 2):268–276.

McAlonan GM, Suckling J, Wong N, Cheung V, Lienenkaemper N, Cheung C, Chua SE (2008): Distinct patterns of grey matter abnormality in high-functioning autism and Asperger's syndrome. J Child Psychol Psychiatry 49:1287–1295.

McAlonan GM, Cheung C, Cheung V, Wong N, Suckling J, Chua SE (2009): Differential effects on white-matter systems in high-functioning autism and Asperger's syndrome. Psychol Med 39:1885–1893.

McCann J, Peppé S (2003): Prosody in autism spectrum disorders: a critical review. Int J Lang Commun Disord 38:325–350.

McCleery JP, Ceponiene R, Burner KM, Townsend J, Kinnear M, Schreibman L (2010): Neural correlates of verbal and nonverbal semantic integration in children with autism spectrum disorders. J Child Psychol Psychiatry 51:277–286.

Mechelli A, Friston KJ, Frackowiak RS, Price CJ (2005): Structural covariance in the human cortex. J Neurosci 25:8303–8310.

Mengotti P, D'Agostini S, Terlevic R, De Colle C, Biasizzo E, Londero D, Ferro A, Rambaldelli G, Balestrieri M, Zanini S, Fabbro F, Molteni M, Brambilla P (2011): Altered white matter integrity and development in children with autism: a combined voxel-based morphometry and diffusion imaging study. Brain Res Bull 84:189–195.

Moher D (2010): Corrigendum to preferred reporting items for systematic reviews and meta-analyses: The PRISMA statement. Int J Surg 8:336–341.

Mori S, Oishi K, Jiang H, Jiang L, Li X, Akhter K, Hua K, Faria AV, Mahmood A, Woods R, Toga AW, Pike GB, Neto PR, Evans A, Zhang J, Huang H, Miller MI, van Zijl P, Mazziotta J (2008): Stereotaxic white matter atlas based on diffusion tensor imaging in an ICBM template. Neuroimage 40:570–582.

Mundy P (2003): Annotation: The neural basis of social impairments in autism: The role of the dorsal medial-frontal cortex and anterior cingulate system. J Child Psychol Psychiatry 44:793–809.

Noriuchi M, Kikuchi Y, Yoshiura T, Kira R, Shigeto H, Hara T, Tobimatsu S, Kamio Y (2010): Altered white matter fractional anisotropy and social impairment in children with autism spectrum disorder. Brain Res 1362:141–149.

Nosarti C, Giouroukou E, Healy E, Rifkin L, Walshe M, Reichenberg A, Chitnis X, Williams SC, Murray RM (2008): Grey and white matter distribution in very preterm adolescents mediates neurodevelopmental outcome. Brain 131 (Part 1):205–217.

O'Connor K (2012): Auditory processing in autism spectrum disorder: A review. Neurosci Biobehav Rev 36:836–854.

Oishi K, Zilles K, Amunts K, Faria A, Jiang H, Li X, Akhter K, Hua K, Woods R, Toga AW, Pike GB, Rosa-Neto P, Evans A, Zhang J, Huang H, Miller MI, van Zijl PC, Mazziotta J, Mori S (2008): Human brain white matter atlas: Identification and assignment of common anatomical structures in superficial white matter. Neuroimage 43:447–457.

Pardini M, Garaci FG, Bonzano L, Roccatagliata L, Palmieri MG, Pompili E, Coniglione F, Krueger F, Ludovici A, Floris R, Benassi F, Emberti Gialloreti L (2009): White matter reduced streamline coherence in young men with autism and mental retardation. Eur J Neurol 16:1185–1190.

Persico AM, Bourgeron T (2006): Searching for ways out of the autism maze: Genetic, epigenetic and environmental clues. Trends Neurosci 29:349–358.

Phillips OR, Clark KA, Woods RP, Subotnik KL, Asarnow RF, Nuechterlein KH, Toga AW, Narr KL (2011): Topographical relationships between arcuate fasciculus connectivity and cortical thickness. Hum Brain Mapp 32:1788–1801.

Pina-Camacho L, Villero S, Fraguas D, Boada L, Janssen J, Navas-Sánchez FJ, Mayoral M, Llorente C, Arango C, Parellada M (2012): Autism spectrum disorder: Does neuroimaging support the DSM-5 proposal for a symptom dyad? A systematic review of functional magnetic resonance imaging and diffusion tensor imaging studies. J Autism Dev Disord 42:1326–1341.

Piven J, Palmer P, Jacobi D, Childress D, Arndt S (1997): Broader autism phenotype: Evidence from a family history study of multiple-incidence autism families. Am J Psychiatry 154:185–190.

Polšek D, Jagatic T, Cepanec M, Hof PR, Simić G (2011): Recent developments in neuropathology of autism spectrum disorders. Transl Neurosci 2:256–264.

Pugliese L, Catani M, Ameis S, Dell'Acqua F, Thiebaut de Schotten M, Murphy C, Robertson D, Deeley Q, Daly E, Murphy DG (2009): The anatomy of extended limbic pathways in Asperger syndrome: A preliminary diffusion tensor imaging tractography study. Neuroimage 47:427–434.

Radua J, Mataix-Cols D (2009): Voxel-wise meta-analysis of grey matter changes in obsessive-compulsive disorder. Br J Psychiatry 195:393–402.

Radua J, van den Heuvel OA, Surguladze S, Mataix-Cols D (2010): Meta-analytical comparison of voxel-based morphometry studies in obsessive-compulsive disorder vs other anxiety disorders. Arch Gen Psychiatry 67:701–11.

Radua J, Via E, Catani M, Mataix-Cols D (2011): Voxel-based meta-analysis of regional white-matter volume differences in autism spectrum disorder versus healthy controls. Psychol Med 41:1539–1550.

Raz N, Gunning FM, Head D, Dupuis JH, McQuain J, Briggs SD, Loken WJ, Thornton AE, Acker JD (1997): Selective aging of the human cerebral cortex observed in vivo: Differential vulnerability of the prefrontal gray matter. Cereb Cortex 7:268–282.

Reiss AL, Abrams MT, Singer HS, Ross JL, Denckla MB (1996): Brain development, gender and IQ in children. A volumetric imaging study. Brain 119 (Part 5):1763–1774.

Rizzolatti G, Craighero L (2004): The mirror-neuron system. Annu Rev Neurosci 27:169–192.

Rizzolatti G, Fabbri-Destro M (2010): Mirror neurons: From discovery to autism. Exp Brain Res 200:223–237.

Robbins TW (1990): The case of frontostriatal dysfunction in schizophrenia. Schizophr Bull 16:391–402.

Rojas DC, Peterson E, Winterrowd E, Reite ML, Rogers SJ, Tregellas JR (2006): Regional gray matter volumetric changes in autism associated with social and repetitive behavior symptoms. BMC Psychiatry 6:56.

Ruef A, Curtis L, Moy G, Bessero S, Badan BM, Lazeyras F, L'vblad KO, Haller S, Malafosse A, Giannakopoulos P, Merlo M (2012): Magnetic resonance imaging correlates of first-episode psychosis in young adult male patients: Combined analysis of grey and white matter. J Psychiatry Neurosci 37:305–312.

Rutter ML (2011): Progress in understanding autism: 2007–2010. J Autism Dev Disord 41:395–404.

Sacco R, Curatolo P, Manzi B, Militerni R, Bravaccio C, Frolli A, Lenti C, Saccani M, Elia M, Reichelt KL, Pascucci T, Puglisi-Allegra S, Persico AM (2010): Principal pathogenetic components and biological endophenotypes in autism spectrum disorders. Autism Res 3:237–252.

Santos M, Uppal N, Butti C, Wicinski B, Schmeidler J, Giannakopoulos P, Heinsen H, Schmitz C, Hof PR (2011): Von Economo neurons in autism: a stereologic study of the frontoinsular cortex in children. Brain Res 1380:206–217.

Schwartz M, Shechter R (2010): Protective autoimmunity functions by intracranial immunosurveillance to support the mind: The missing link between health and disease. Mol Psychiatry 15:342–354.

Shannon P, Markiel A, Ozier O, Baliga NS, Wang JT, Ramage D, Amin N, Schwikowski B, Ideker T (2003): Cytoscape: A software environment for integrated models of biomolecular interaction networks. Genome Res 13:2498–2504.

Solomon M, Ozonoff SJ, Ursu S, Ravizza S, Cummings N, Ly S, Carter CS. (2009): The neural substrates of cognitive control deficits in autism spectrum disorders. Neuropsychologia 47:2515–2526.

Spencer MD, Moorhead TW, Lymer GK, Job DE, Muir WJ, Hoare P, Owens DG, Lawrie SM, Johnstone EC (2006): Structural correlates of intellectual impairment and autistic features in adolescents. Neuroimage 33:1136–1144.

Thompson PM, Giedd JN, Woods RP, MacDonald D, Evans AC, Toga AW (2000): Growth patterns in the developing brain detected by using continuum mechanical tensor maps. Nature 404:190–193.

Toal F, Daly EM, Page L, Deeley Q, Hallahan B, Bloemen O, Cutter WJ, Brammer MJ, Curran S, Robertson D, Murphy C, Murphy KC, Murphy DG (2010): Clinical and anatomical heterogeneity in autistic spectrum disorder: a structural MRI study. Psychol Med 40:1171–1181.

Uddin LQ, Menon V (2009): The anterior insula in autism: underconnected and under-examined. Neurosci Biobehav Rev 33:1198–1203.

Van den Heuvel OA, Mataix-Cols D, Zwitser G, Cath DC, van der Werf YD, Groenewegen HJ, van Balkom AJ, Veltman DJ (2011): Common limbic and frontal-striatal disturbances in patients with obsessive compulsive disorder, panic disorder and hypochondriasis. Psychol Med 41:2399–2410.

Van Haren NE, Hulshoff Pol HE, Schnack HG, Cahn W, Mandl RC, Collins DL, Evans AC, Kahn RS (2007): Focal gray matter changes in schizophrenia across the course of the illness: A 5-year follow-up study. Neuropsychopharmacology 32:2057–2066.

Waiter GD, Williams JH, Murray AD, Gilchrist A, Perrett DI, Whiten A (2005): Structural white matter deficits in high-functioning individuals with autistic spectrum disorder: A voxel-based investigation. Neuroimage 24:455–461.

Xu L, Pearlson G, Calhoun VD (2009): Joint source based morphometry identifies linked gray and white matter group differences. Neuroimage 44:777–789.

Zamboni G, Huey ED, Krueger F, Nichelli PF, Grafman J (2008): Apathy and disinhibition in frontotemporal dementia: Insights into their neural correlates. Neurology 71:736–742.